ARCTEC CANADA LIMITED

MODELLING OF MOLTEN METAL PENETRATION INTO A PARTICULATE LAYER

DSS FILE NO. 3SQ.23440-5-9238

CONTRACT SERIAL NO. OSQ85-00341
CONTRACTOR: ARCTEC CANADA LTD.
CONTRACT REQ'N NO. 23440-5-9238

JANUARY 1988

SUBMITTED BY:

ARCTEC CANADA LIMITED
311 Legget Drive,
Kanata, Ontario.
K2K 1Z8

80pp

MICROMEDIA

90-05663//

TABLE OF CONTENTS

Page

Summary

1. INTRODUCTION.....1

2. OBJECTIVE.....9

3. METHODOLOGY.....10

4. RESULTS.....28

5. DISCUSSION.....42

6. CONCLUSIONS.....48

REFERENCES.....49

APPENDIX A: PREDICTION OF VELOCITY AND TEMPERATURE FIELDS FOR CONFINED FLUID FLOWS

APPENDIX B: COMPUTER PROGRAM SOLA

SUMMARY

A model was developed to define attributes to predict the penetration of molten alloy into a particulate layer. The present study considers tungsten carbide as the powder and steel as the molten alloy. Results are presented for flow of molten steel through the powder bed under three gauge pressures. A Peclet number is used to estimate the relative magnitude of heat transfer due to convection and conduction in the axial direction, from which an eddy conductivity value is calculated.

Résumé

Un modèle a été développé à fin de définir les attributs pour prédire la pénétration d'un alliage en fusion dans une couche de particules en poudre. A présent, l'étude considère le carbure de tungstène pour la poudre et l'acier pour l'alliage fondu. Les résultats pour un flux d'acier en fusion traversant une couche de poudre à trois pressions différentes, sont présentés. Un numéro Peclet a été utilisé pour estimer l'empleur du transfer calorifique dû à la convection ainsi qu' à la conduction dans la direction axial. A partir de ceçi, une valeur pour la conductivité en tourbillou est calculé.

1. INTRODUCTION

Toughness and resistance to abrasion are the two most important properties needed for parts such as digger teeth. These two requirements conflict. However, by providing an abrasion resistant surface layer and a tough core, the desired combination of properties can be achieved.

The basic technique to obtain a toughened surface matrix is to provide a layer of abrasion resistant grains in a mold casting. On pouring, the molten metal permeates the layer to give a bonded abrasion-resistant surface.

The schematics of the technique are shown in Figure 1. For the system in question, the development of a mathematical model based on theoretical considerations is greatly complicated by the transient nature of the problem and by the fact that many interacting physical phenomena are involved. For example, the heat flux out of the mold determines both the solidification rate of the molten metal and dissolution rate of the particles, which in turn affect the flow of liquid metal through the powder bed. Fluid mechanics, in turn, defines the nature of the flow, which affects heat transfer characteristics.

A procedure for cast-in-place hardfacing of castings has been developed at the Physical Metallurgy Research Laboratories [1]. In this method, the molten metal is poured into a sand mold and is drawn by vacuum into a layer of abrasion-resistant powder (or grains) placed on a wall of the mold cavity. The infiltrated powder provides a metallurgically bonded, abrasion resistant coating on the casting. AISI 1020 and 4340 steels, austenitic magnanese steels and both grey and ductile cast irons have been successfully coated with CrC, WC and WC-10% Co powders [1].

The objective of this undertaking was to define attributes for reaching an understanding of what physical phenomena are important for predicting the penetration of a molten metal alloy into a particulate layer, as a function of metal temperature and hydrostatic pressure. In order to do this, experiments were performed and the heat equation was solved. However, fluid flow was not analyzed numerically.

There are many physical situations in which the flow of liquids through porous materials is of concern, including the seepage of water through soil underneath dams and buildings, and fluid flow in packed towers and filtration apparatus.

The porous layer is made up of separate small solid particles. Results [2] indicate the existence of four regimes of flow in porous media, viz:

(1) The Darcy regime where the flow is dominated by viscous forces and the exact nature of the flow is determined by local geometry. This type of flow occurs at Reynolds Number (Re) of less

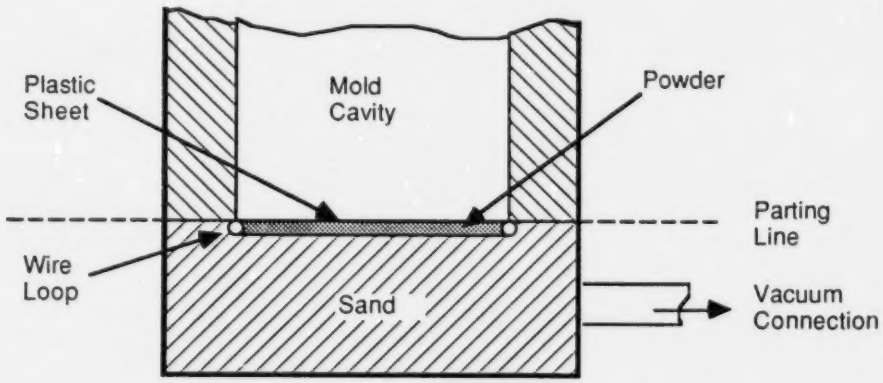

Figure 1 Schematic Diagram of the Technique for Cast-in-place Hardfacing

than 1 and Darcy's law, which states that the flow rate is directly proportional to the pressure gradient, is valid. At Re=1, boundary layers begin to develop near the solid boundaries of the pore.

2) The inertial flow regime lies between Re of 1 to 10, wherein the boundary layers become more pronounced and an "inertial core" appears. The development of the "core" flows outside the boundary layers causes a nonlinear relationship between the pressure gradient and the flow rate.

3) An unsteady laminar flow regime in the range $200 < Re < 350$, which is characterized by laminar wake oscillation for $200 < Re < 300$ followed by vortices in the range $300 < Re < 350$.

4) A highly unsteady and chaotic regime for $Re > 350$ that qualitatively resembles turbulent flow.

In the situation under study, the velocities are usually small and the flow passages are narrow, and hence laminar i.e. regime 1 flow may be reasonably assumed. Because of the complex individual flow passages and their shape, rigorous analysis is not possible.

Henry Darcy performed experiments in the mid 1800's on the flow of water through a pipe packed with sand and postulated that

$$P' = \frac{\mu}{K} V \qquad (1)$$

where P' = negative of the pressure gradients in the direction of flow

V = volume rate of flow per unit area

μ = dynamic viscosity of the fluid

K = a constant of proportionality (permeability of the medium)

In order to relate equation (1) to specific porous media in terms of diameter of the particles, Josef Kozeny improved upon the equation. He considered the porous medium to be made up of separate small solid particles, and the flow to be, broadly speaking, in one direction only: thus, although the fluid flows through a somewhat tortuous path, there is no net flow across the block of material, in any direction, other than the fluid flow direction.

Whatever the actual shape of the individual passages, the overall result is the same as if, in place of the porous material, there were a large number of parallel, identical, capillary tubes with their axes in the flow direction. Kozeny then reasoned that, since the resistance to flow results from the requirement of no slip at any solid boundary, the capillary tubes and the porous medium would be truly equivalent only, if, for a given volume occupied by the fluid, the total surface area of the solid boundaries were the same in each case.

In the porous medium the ratio of the volume of voids (re the spaces between the solid particles) to the total volume is known as the porosity, ε. Thus,

$$\varepsilon = \frac{\text{Volume of voids}}{\text{Volume of voids + Volume of solids}} = \frac{V_v}{V_v + V_s}$$

Therefore,

$$\frac{\text{Volume of voids}}{\text{Total surface area}} = \frac{V_v}{S} = \frac{V_s . \varepsilon}{(1-\varepsilon)S}$$

The corresponding value for a capillary tube of internal diameter d and length l is $(\pi/4)d^2 l/\pi dl = d/4$. Thus if the set of capillary tubes is to be equivalent to the porous medium then each must have an internal diameter

$$d = \frac{4 V_s \varepsilon}{(1-\varepsilon)S}$$

$$= \frac{4 \varepsilon}{(1-\varepsilon).S_o}$$

where S_o = specific surface of the particles (i.e. surface area per unit volume) = $6/d_p$, where d_p = particle diameter

Thus, Equivalent Capillary Tube Diameter,

$$d_e = \frac{2\varepsilon d_p}{3(1-\varepsilon)} \qquad (2)$$

The 'd_p' in equation (2) is based on the assumption of a uniform particle size in the media. However, as suggested [3], the 'd_p' in equation (2) can be replaced by the weighted mean harmonic diameter 'd_h' for porous medium composed of particles that are not uniform in size. That is,

$$d_h = \left[\sum_{i=1}^{n} \frac{fi}{di} \right]^{-1}$$, where fi = mass fraction for particles having diameter di.

If all the flow passages in the porous media are in the direction of flow, the mean velocity of the fluid would be $\bar{u}/\varepsilon$ (because only a fraction ε of the total cross section is available for flow). The actual paths, however, are sinuous and have an average length le, which is greater than l, the thickness of the porous material. The mean velocity in the passages is therefore greater than if the passages were straight, and is given by $(\bar{u}/\varepsilon/le/l)$. Flow at this mean velocity in capillary tubes of length le would require a drop of piezometric pressure P', given by

$$\frac{P'}{le} = \frac{32\mu}{d_p^2} \frac{\bar{u}le}{\varepsilon l} \qquad (3)$$

Rearrangement of equation (3) gives,

$$\bar{u} = \frac{P'}{l.\alpha\mu k(S_o)^2} \qquad (4)$$

where, $\alpha = \dfrac{(1-\varepsilon)^2}{\varepsilon^3}$

k = Kozeny-Carman Constant

$$= \frac{d_p^2 P'}{36\mu\bar{u}d} \qquad (5)$$

The permeability K is related the Kozeny-Carman Constant by

$$K = (kS_o^2\alpha)^{-1} \qquad (6)$$

'K' depends to some extent on ε and it depends also on the arrangement of particles, their shape and their range. Nevertheless, experiment shows that for many materials K ranges only from about 4.0 to 6.0.

Because the solid particles touch each other, part of the total surface area S is ineffective in causing resistance to flow - especially if there are flat-sided particles. Moreover, any re-entrant parts of the surface make little, if any, contribution to the resistance. Consequently, S would be better defined as the effective surface area. In practice, however, the difference between the total and the effective surface area is absorbed into the experimentally determined value of k.

The usual packing of spherical particles into a mold can be approximated by an orthorhombic arrangement giving a porosity of about 40% [4]. Irrespective of the packing arrangement and total porosity of the bed, the smallest pore will be the interstitial site formed by three touching spheres on a given cross-sectional plane, as shown in Figure 2. The differential fluid element will have to penetrate through such constrictions, to cause the penetration of the particulate layer.

The ability of liquid metals and alloys to flow along channels of defined dimensions is an important factor influencing casting practice. This ability can be quantified for given casting conditions as the extent and duration of flow identified respectively with the terms casting fluidity and fluid life. Although there is a substantial amount of information concerning the effect of casting variables, especially on casting fluidity, only limited effort has been expended to compare qualitatively results with predictions from theoretical models of the conditions that lead to cessation of flow [5-9].

Wetting characteristics of the liquid-solid system is an important parameter when considering the flow of a liquid phase through a porous medium [4]. Two extreme cases might exist:

i) the liquid wets the medium

ii) the liquid is nonwetting

For the case of wetting liquids, the surface tension forces enhance flow, such as in the case of water flow through soils. These types of flow problems can be tackled by Darcy, Kozeny-Carman or Poiseuille equations. For nonwetting liquids, the surface tension forces must be overcome for flow to be initiated. The pressure required to force the liquid through a constriction can be solved by Laplace's equation [9].

The other important physical phenomenon is the dissolution kinetics of the particles in the molten alloy and the associated depression of the freezing point of the molten alloy. Studies done by Argyropoulos et al [10] on ferro-alloy additions have shown that, ferro-alloys, at least, can be grouped into two major classifications, viz; Class I in which the melting ranges are below that of the steel and Class II, in which the melting ranges are above that of steel.

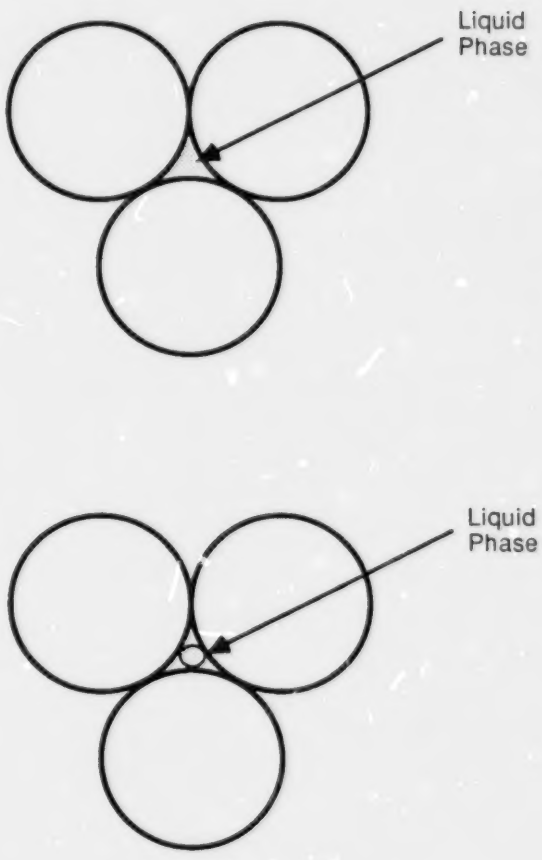

Figure 2 Model of Triangular Orifice and Liquid Phase Geometries

In terms of the prediction of freezing time of the steel in porous medium, the dissolution kinetics could be a major consideration in terms of:

i) freezing point

ii) dissolution rate, which will dictate the interaction between heat and fluid flow.

In the present study, the dissolution aspect has not been considered.

2. OBJECTIVE

The objective of this work was to define attributes for a basic model to predict the penetration of a molten alloy into a particulate layer.

3. METHODOLOGY

3.1 Assumptions

i) The porous bed can be effectively replaced by a bank of capillary tubes and the flow is in one direction only. Thus, although the fluid follows a somewhat tortuous path through this material, there is no net flow across the block of material, except in the axial direction. This assumption was necessary in order to simplify the flow of fluid through a tortuous path, and still be able to model the effect of particle size on heat and fluid flow through the porosity factor.

ii) Wetting characteristics of the fluid-solid system is an important variable when flow of a fluid phase through a porous medium is of concern. For the case of wetting fluids, as has been assumed in this study, the effect of surface tension forces is small. This assumption was made in order to be able to use the various governing equations postulated by Darcy, Kozeny and Carman, etc. for laminar flow of fluid through capillary tubes and simplify the analysis to a great extent.

iii) The riser is filled instantaneously, and then the molten metal penetrates through the porous bed and subsequently freezes. This assumption essentially implies that there is no heat loss from the fluid until it comes in contact with the porous bed, at which point the temperature of the fluid is at the pouring temperature. This assumption was necessary in order to isolate the porous bed and the fluid flow from the rest of the system.

iv) Powder particles do not dissolve in the molten metal. This assumption was made so that a simple model of heat and fluid flow can be developed without getting into the complexity of 'moving boundary' problems, and effect of dissolution of particles on freezing of fluid.

v) The flow is laminar and the mean velocity profile is rectangular instead of parabolic.

vi) Viscosity of the fluid is constant, i.e. it does not depend on temperature.

vii) The latent heat of solidification (272 kJ/kg) is assumed to evolve linearly over the two-phase region between the liquidus and solidus temperatures. The latent heat is taken into account in the model through the respective heat contents.

viii) Any effects of heat transfer through the scale layer is ignored, i.e. thermal contact resistance at the fluid/solid interface is ignored.

ix) The 'fountain flow' effect near the solidifying meniscus for the flowing fluid is ignored.

x) Any heating due to radiation or convection ahead of the leading edge of the flow front is not considered in the present study.

3.2 Model Considerations

The system in consideration is shown schematically in Figure 3. For analysis a capillary tube flow model is adopted. The system can be represented as shown in Figure 4.

Since the riser contains the bulk of the molten metal, the fluid temperature essentially remains constant at the pouring temperature (assumption (iii)). Because of assumption (i), we can analyze a single capillary tube system to study the heat transfer and fluid flow characteristics. This system can be analyzed as a 2-dimensional axysymmetric tube model.

The fluid is allowed to flow between the powder wall passages, heat is lost radially as well as axially to the surroundings as the fluid flows downwards and subsequently freezes.

If we assume that the capillary pore is instantaneously filled by the molten metal, then there is no axial heat conduction, but heat is only lost radially. With this assumption, one can take a thin slice and analyze for radial heat flow only. The freezing time thus calculated will be the lower bound of the solution, i.e. this will give the fastest cooling time. This model is termed 'cross-sectional model' and is shown in Figure 5.

The 'axial flow model' attempts to incorporate the progress of fluid front as it flows down the tube, looses heat axially as well as radially and subsequently freezes. This model is shown schematically in Figure 6. Because of symmetry along the axial direction, only one half of the tube is modelled.

The liquidus and solidus temperatures were calculated from the composition data using the following empirical equations [11].

$$T_{Liq} = 1537 - 88(\%C) - 25(\%S) - 5(\%Cu) - 8(\%Si) - 5(\%Mn) - 2(\%Mo) - 4(\%Ni) - 1.5(\%Cr) - 18(\%Ti) - 2(\%V) - 30(\%P) \quad (7)$$

$$T_{Sol} = 1535 - 200(\%C) - 12.3(\%Si) - 6.8(\%Mn) - 124.5(\%P) - 183.4(\%S) - 4.3(\%Ni) - 1.4(\%Cr) - 4.1(\%Al) \quad (8)$$

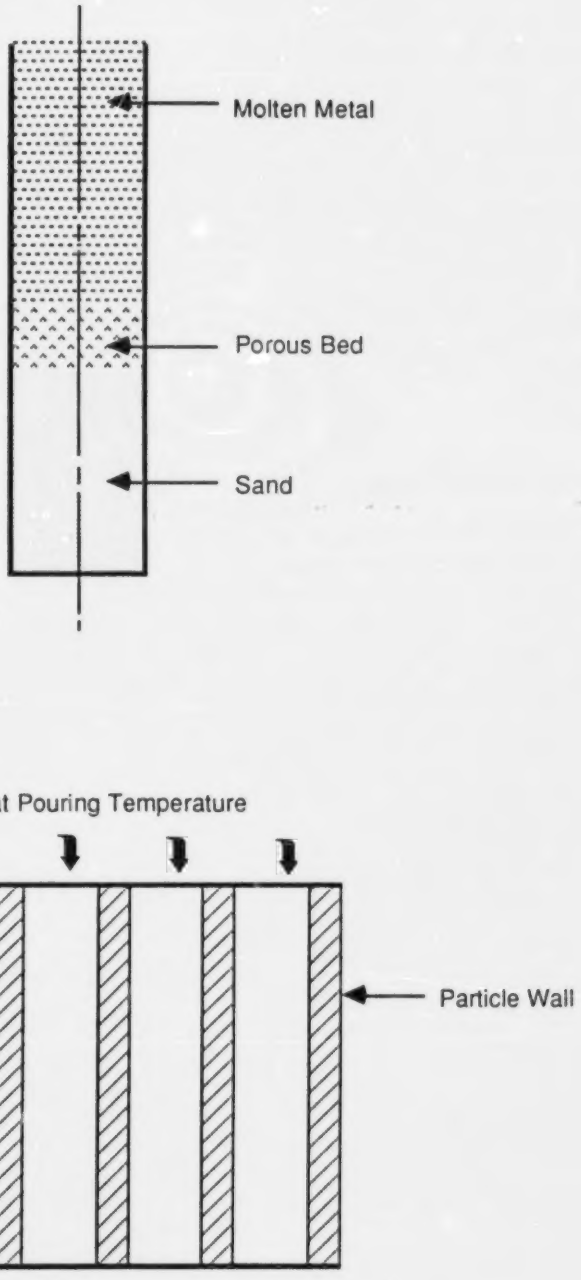

Figure 3 Molten Metal Flow Through the Porous Bed and Capillary Flow Model

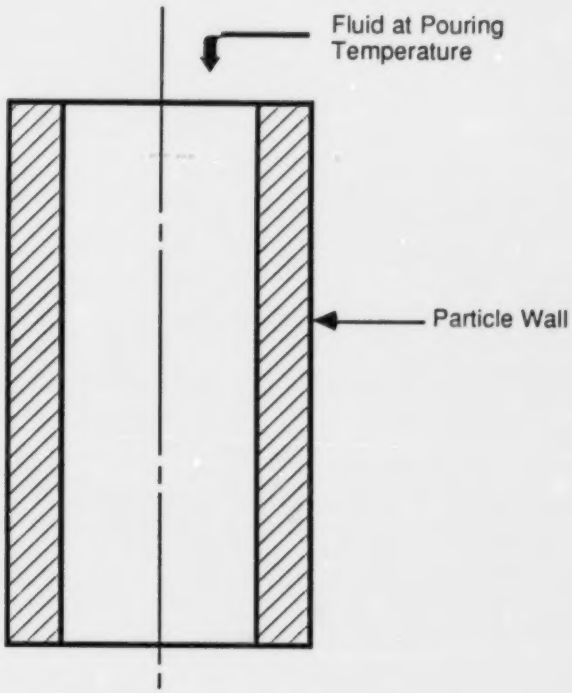

Figure 4 Single Capillary Tube System

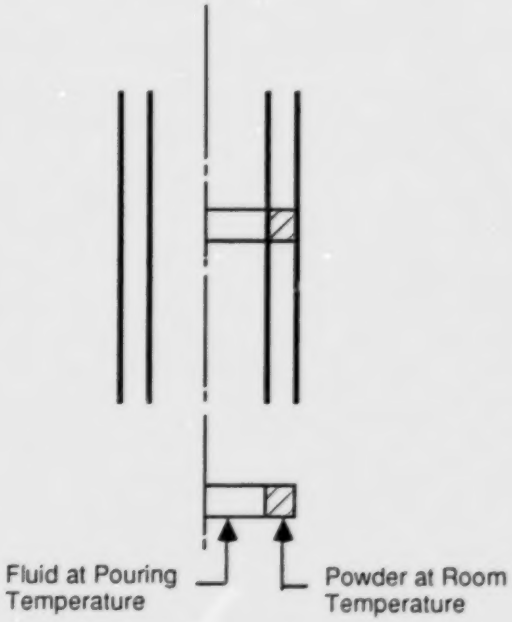

Figure 5 Cross Sectional Model

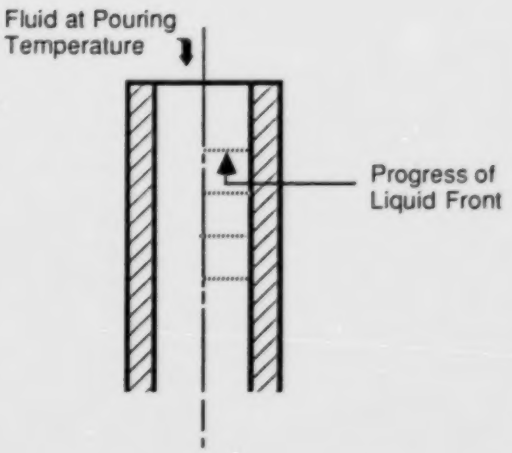

Figure 6 Axial Model With Fluid Flow

The governing equation for heat conduction within the steel and the mold is given by:

$$\frac{\partial}{\partial x}\left(K\frac{\partial T}{\partial x}\right) + \frac{\partial}{\partial y}\left(K\frac{\partial T}{\partial x}\right) = \rho c\frac{\partial T}{\partial t} \qquad (9)$$

This is the equation that was solved for the 'cross-sectional' and 'axial flow' models using the Finite Element computer program 'ASGARD'.

For the 'Axial Flow Model', we assume that the molten fluid with a given temperature distribution flows instantaneously for a very small distance Δl and is retained for Δt seconds, and this process is repeated. This model may be approximated to the metal flow with a constant velocity $V = \Delta l/\Delta t$. The heat absorbed during the time duration Δt by the cylindrical mold of length Δl, which is in contact with the same length of the tip can be calculated. However, 'ASGARD' did not have the capability of simulating the step wise flow of fluid, as described.

In order to do this, the 'ASGARD' program was modified so that the above described simulation can be performed. Along the interface, the nodes on the fluid and capillary tube interface were assumed to have sectorial symmetry, and 2 node bar elements were used. These bar elements can only conduct heat and have no heat storing capacity. The system is shown schematically in Figure 7 and 8. For each time step (calculated according to the length of each element and the velocity), the finite elements were connected in a pre-defined manner. In this way, the step wise flow of fluid in the capillary was simulated.

Results of these two models showed that the molten metal was losing heat to the particle walls much faster because of high temperature gradients and also because of the fact that effective heat flow area of the particles was larger than the cross-sectional area of the molten metal. Because of this, the penetration was smaller.

It was postulated that the heat flow in the axial direction due to the velocity is significant. A fully coupled fluid flow-heat transfer analysis capable of simulating the 'filling' of the capillary tube would be ideal. Instead, we attempted to simplify the situation to some extent as follows.

The energy equation can be written for one dimensional geometry as

$$K\frac{\partial^2 T}{\partial x^2} - V\frac{\partial T}{\partial x} = \rho c\frac{\partial T}{\partial t} \qquad (10)$$

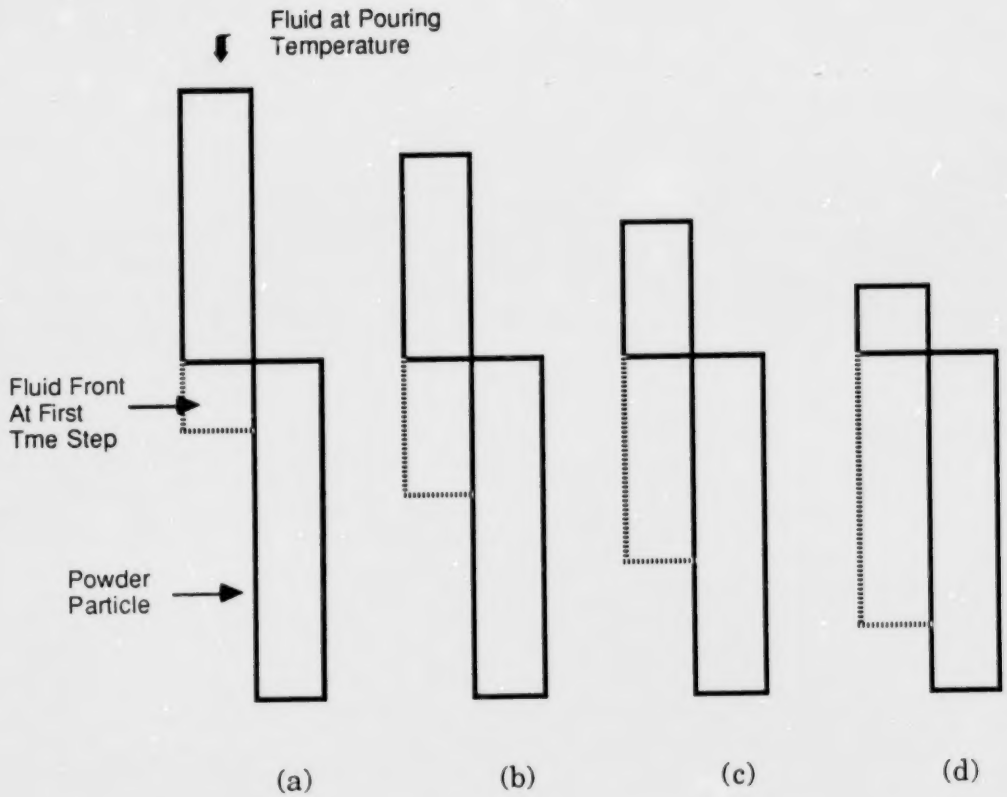

Figure 7 Flow of Fluid with each Time Step

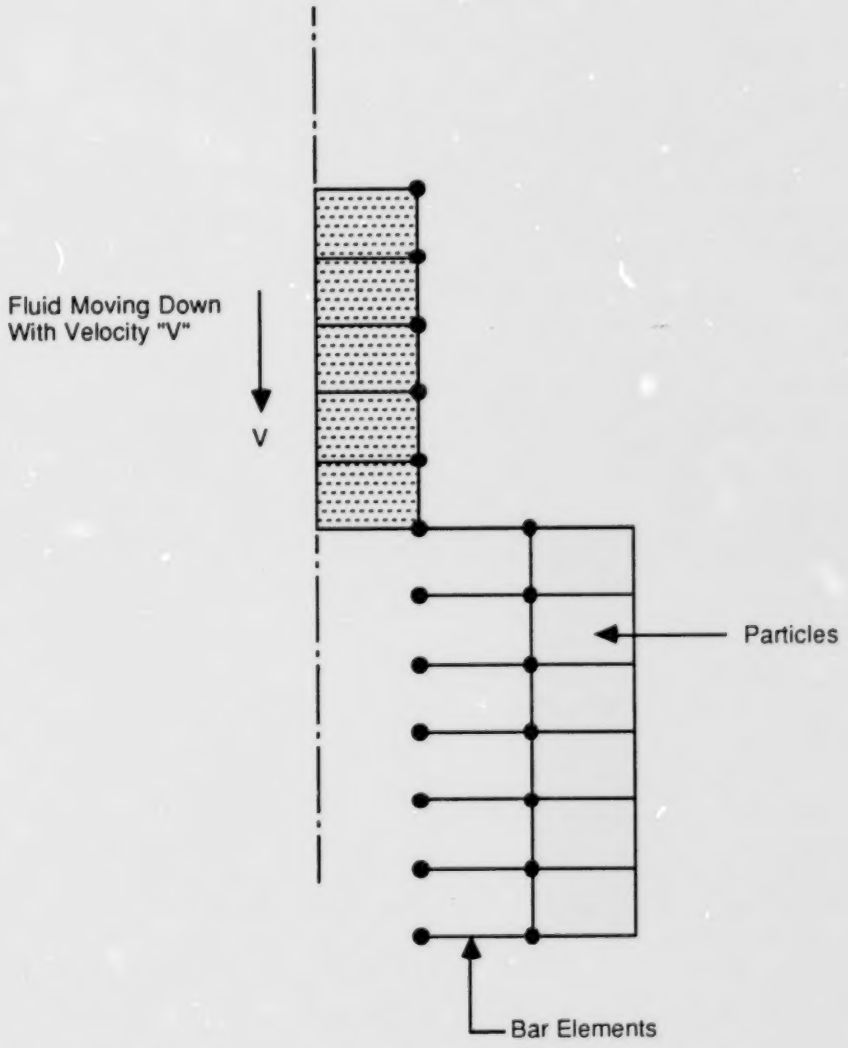

Figure 8 Bar Elements With Sectorial Symmetry to Simulate Flow of Molten Metal

in which,

K = thermal conductivity
V = velocity in the axial direction
ρc = volumetric specific heat

$\frac{\partial^2 T}{\partial x^2}$ = curvature of the temperature distribution curve

$\frac{\partial T}{\partial x}$ = slope of the temperature distribution curve

If the effect of the velocity term on the temperature distribution is known, or estimated, then an effective 'eddy conductivity' value can be calculated. Coming back to the 'axial flow model', we can then incorporate the anisotropic thermal conductivity values to calculate the penetration of the molten metal into the particulate layer. This was accomplished by obtaining a copy of the program 'SOLA' and modifying it to take into account the transient heat flow solution coupled to transient fluid flow solution. 'SOLA' is a finite difference computer program developed at Los Alamos Scientific Laboratory [12, 13, 14]. The details of the program and a complete listing is given in Appendix A.

The heat transfer by convection and heat transfer by conduction can be characterized by Peclet number, which is

$$P_e = \frac{\rho_c V l}{K}$$

If the above ratio is greater than unity, the heat transfer by convection dominates.

After the 'eddy conductivity' values were obtained, the 'axial flow' model was used to calculate the transient temperature field. When a node at the interface reached a temperature equal to the solidus temperature (≈ 1450°C), it was concluded that the solidification had started. The depth to which the fluid flowed before the beginning of solidification, is termed as 'penetration due to the flow (PF)' and is shown in Figure 9.

At this stage, the cross-sectional model was utilized - in which the solidification front was monitored (latent heat effects) and the solidification speed was calculated. The radius of the channel divided by the solidification speed gave a 'time' during which additional fluid can flow down. This penetration is termed as 'penetration during solidification' and is shown in Figure 10. The total penetration is the sum of 'penetration due to the flow' and 'penetration during solidification (P_S), i.e.

$$P_T = P_F + P_S \qquad (11)$$

This is shown schematically in Figure 11.

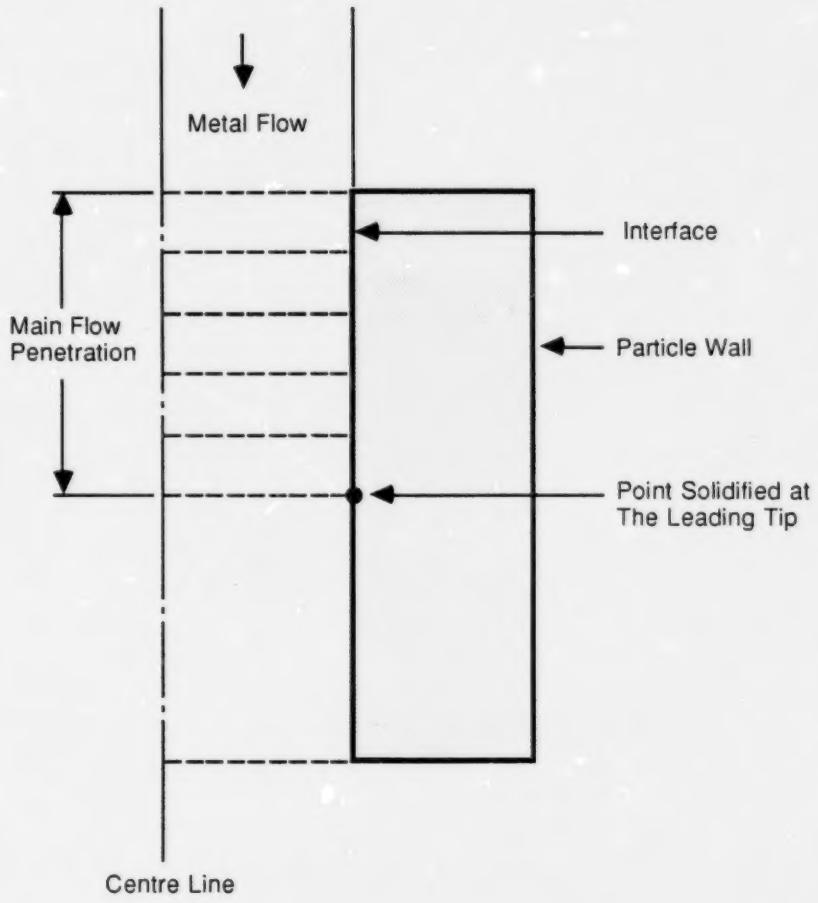

Figure 9 Schematic of Main Flow Penetration

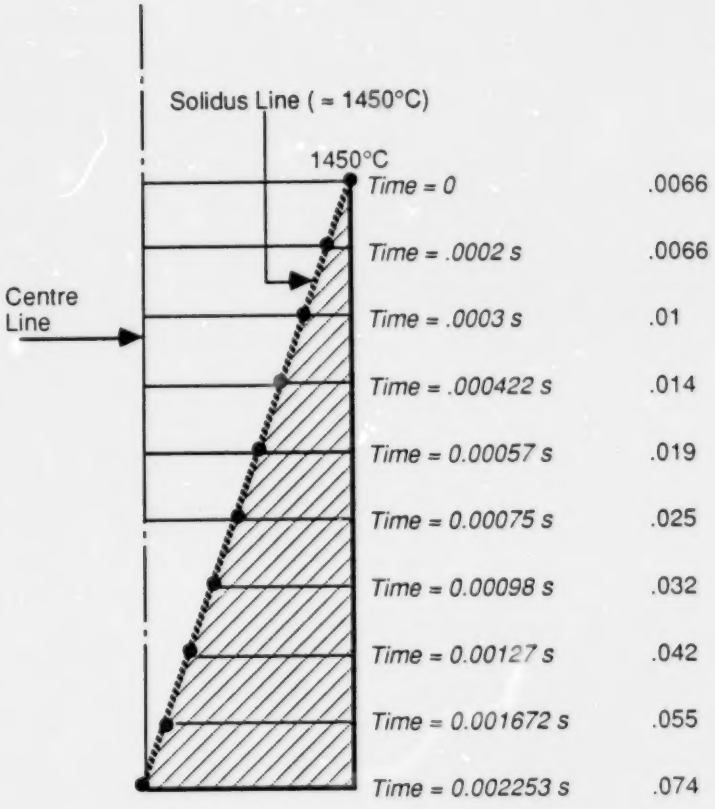

Figure 10 Schematic of Penetration During Solidification

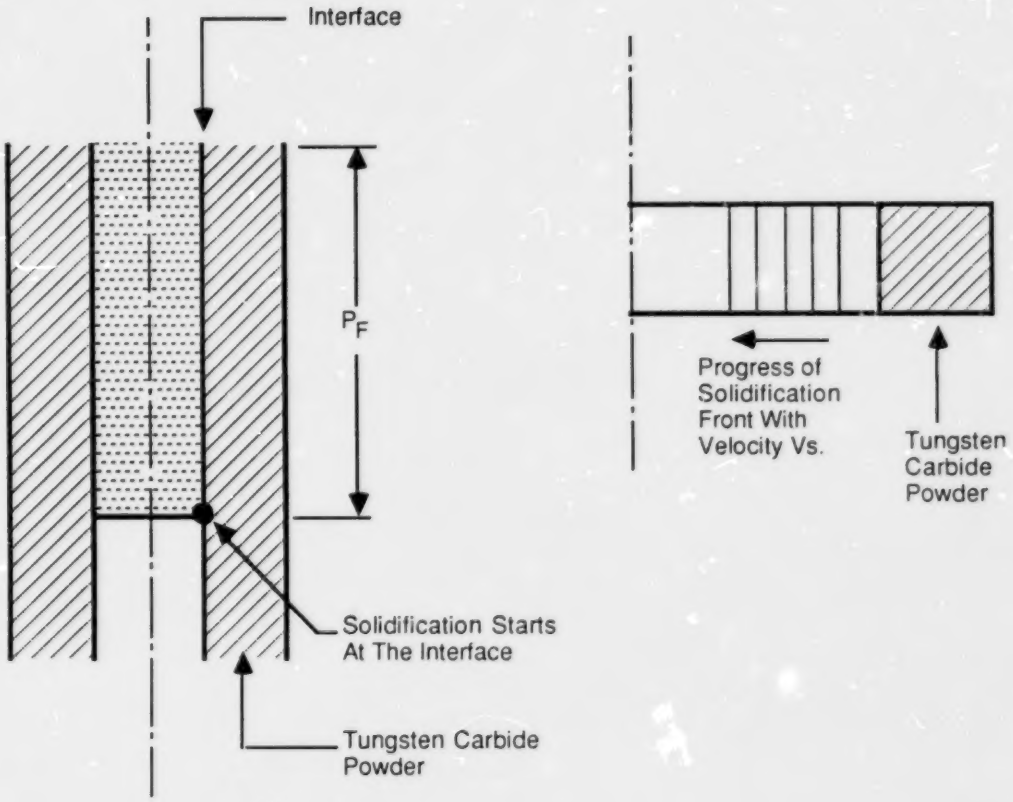

Time to Complete Solidification (ts) = Channel Radius/Vs
So, P_F = ts x Fluid Velocity (V)

Total Penetration, P_T = Penetration due to fluid flow (P_F) +
Penetration during solidification (Ps)

Figure 11 Calculation of Total Penetration

3.3 Experimental

In order to estimate the effect of particle size, viscosity etc. on the fluid velocity and pressure drop, a 'fluid flow apparatus' was designed and built. Glass beads of 1, 2, 3 and 4 mm diameter were used. Two grades of tungsten carbide particles (coarse and fine) were obtained from PMRL, Canmet. Fluids of three different viscosities (water, light oil, heavy oil) were used as the test fluids.

The porous medium (beads or tungsten powder) was held in the fluid apparatus with a fine mesh. The bottom of the apparatus was attached to a vacuum pump which could control the pressure from atmospheric (101.3 kPa) down to 8 kPa (absolute pressure). A vacuum relief valve maintained a constant vacuum pressure in the apparatus. The pressure at two points in the porous medium was measured using strain gauge type pressure transducers. The velocity of the fluid flow through the beads was determined by the volumetric flow rate and the cross sectional area of the jar, $1.695 \pm 0.005 \times 10^{-3}$ m^2. The test set up is shown schematically in Figure 12.

Using glass beads, three liquids were tested: tap water; shell tellus 32, a light oil; and an SAE 40 oil. Approximate viscosities for these liquids are given in Table 1. The results of the tests with the beads are given in Table 2.

Tap water was used in combination the coarse tungsten powder. The results of the test are given in Table 3. It was not possible to take any measurements with the fine tungsten powder since during the three attempted tests the powder completely clogged the filter. The clogging was so complete that almost a full vacuum could be held using a 25 mm layer of fine tungsten powder on top of the filter.

The kinematic viscosity of water and molten steel are assumed to be of the same order of magnitude (Table 1). As such the experimental results for tests with water are equally applicable for the molten steel system.

The porosity of the glass beads was measured and found to be 31% for the 1 and 2 mm beads, 31.2% for the 3 mm beads and 32.2% for the 4 mm beads. The diameter of the beads was also measured and while nominal diameters are 1, 2, 3 and 4 mm, the actual values were 1.2, 2.0, 2.93 and 3.91 mm. Actual diameter values are used in the calculation but nominal values are used to identify the beads.

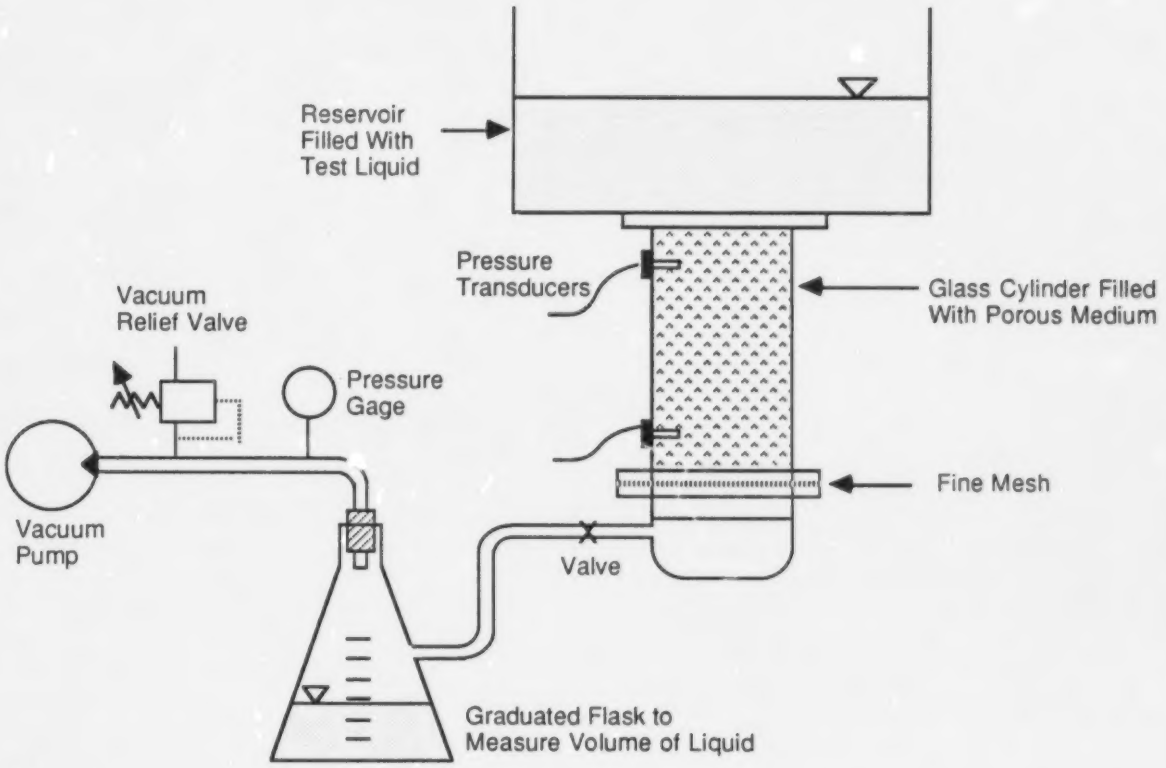

Figure 12 Apparatus For Measuring Flow Through Porous Media

TABLE 1

VISCOSITIES OF VARIOUS FLUIDS

FLUID	DYNAMIC VISCOSITY (Ns/m^2)	KINEMATIC VISCOSITY (m^2/s)	DENSITY (kg/m^3)
Water (22°C)	$.961 \times 10^{-3}$	$.961 \times 10^{-6}$	1000
Tellus 32	69.2×10^{-3}	80×10^{-6}	865.3
SAE 40	430×10^{-3}	500×10^{-6}	860
Steel (Molten)	5×10^{-3}	6.9×10^{-6}	

TABLE 2

TESTS WITH GLASS BEADS

BEAD SIZE	LIQUID	PRESSURE Δp kPa	GAUGE PRESSURE kPa	PREDICTED VELOCITY $\bar{u}_p$ m/s	MEASURED VELOCITY $\bar{u}_m$ m/s	$\bar{u}_m/\Delta p \times 10^{-3}$ m/s/kPa
1.20	Water	10.2	34	0.0574	0.0761	7.45
		11.6	34	0.0656	0.0788	6.80
		7.9	34	0.0447	0.0664	8.42
		13.0	67	0.0737	0.0909	6.99
		13.3	67	0.0754	0.1047	7.86
2.00	Water	7.7	34	0.1211	0.0785	10.20
		8.0	34	0.1260	0.0891	11.14
		8.4	34	0.1318	0.0918	10.97
		13.7	67	0.2163	0.1280	9.32
		15.2	67	0.2396	0.1274	8.37
2.93	Water	8.7	80	0.3008	0.1298	14.92
		8.9	80	0.3098	0.1192	13.39
		7.1	44	0.2450	0.1097	15.52
		6.6	44	0.2280	0.1056	16.05
3.91	Water	8.6	78	0.6021	0.1770	20.53
		6.2	78	0.4339	0.1369	22.04
		6.3	47	0.4379	0.1369	21.83
		6.0	47	0.4205	0.1257	20.87
		3.2	15	0.2221	0.0850	26.72
		3.5	15	0.2435	0.0879	25.19
2.00	Light Oil	38.4	60	0.0084	0.0206	0.54
		37.8	60	0.0083	0.0201	0.53
		22.1	60	0.0048	0.0206	0.93
		17.6	50	0.0038	0.0107	0.61
		16.8	50	0.0037	0.0105	0.63
		16.0	50	0.0035	0.0101	0.63
		9.2	15	0.0020	0.0125	1.36
		9.2	15	0.0020	0.0117	1.27
		8.8	15	0.0019	0.0129	1.46
		8.8	15	0.0019	0.0125	1.42
2.93	Light Oil	9.5	24	0.0046	0.0183	1.92
		17.1	50	0.0082	0.0312	1.82
		12.4	27	0.0060	0.0224	1.81
		12.6	27	0.0060	0.0219	1.74

TABLE 2 (Cont'd)

BEAD SIZE	LIQUID	PRESSURE Δp kPa	GAUGE PRESSURE kPa	PREDICTED VELOCITY $\bar{u}_p$ m/s	MEASURED VELOCITY $\bar{u}_m$ m/s	$\bar{u}_m/\Delta p \times 10^{-3}$ m/s/kPa
2.00	SAE 40	21.9	67	0.0041	0.0024	0.11
		32.0	67	0.0068	0.0040	0.13
		27.8	50	0.0058	0.0034	0.12
		29.7	50	0.0057	0.0034	0.11
		21.8	27	0.0034	0.0020	0.09
2.93	SAE 40	13.8	27	0.0011	0.0030	0.22
		13.8	27	0.0011	0.0028	0.20
		13.7	27	0.0011	0.0029	0.21
		13.4	27	0.0010	0.0034	0.25
		13.1	27	0.0010	0.0030	0.23
		13.1	27	0.0010	0.0030	0.23
		24.8	50	0.0019	0.0048	0.20
		23.3	50	0.0018	0.0045	0.19
		24.4	50	0.0019	0.0046	0.19
		23.7	50	0.0018	0.0059	0.25
		28.7	67	0.0022	0.0057	0.20
		29.4	67	0.0023	0.0058	0.20
		28.7	67	0.0022	0.0065	0.23
3.91	SAE 40	12.8	27	0.0020	0.0050	0.39
		12.8	27	0.0020	0.0045	0.36
		12.2	27	0.0019	0.0043	0.35
		21.4	50	0.0033	0.0086	0.40
		21.4	50	0.0033	0.0085	0.40
		21.0	50	0.0033	0.0077	0.37

TABLE 3

TEST WITH COARSE TUNGSTEN POWDER

LIQUID (kPa)	GAUGE PRESSURE (kPa)	Δp	Q (l/s)	$\bar{u}_m$	$\bar{u}_m/\Delta p \times 10^{-3}$ (m/s/kPa)
water	50	9.2	0.0336	0.0198	2.15
	50	12.0	0.0353	0.0208	1.73
	50	14.1	0.0352	0.0208	1.48
	67	14.2	0.0484	0.0286	2.01
	67	14.7	0.0449	0.0265	1.80
	67	19.3	0.0479	0.0283	1.47
	87	18.0	0.0577	0.0340	1.89
	87	21.0	0.0534	0.0315	1.50
	87	16.6	0.0568	0.0335	2.02

Pressure drop measured over 0.031m.

4. RESULTS

Experimental results were obtained for glass beads of various diameters with water at three pressures of 50, 67 and 87 kPa.

Figure 13 shows the plot of measured velocities and the predicted velocities from equation (4). As can be seen, the measured velocities are a linear function of the predicted velocity. If a straight line is fitted through the points in Figure 10, the slope of the line in water would be about 0.3; in light oil about 4.0; and in SAE 40 oil about 3.0. Ideally the slope should be 1.0. Although the values of viscosity used in the calculation are only approximate they could not account totally for the discrepancy. Further tests should be conducted to determine the relationships of liquid properties to the pressure loss.

In Figure 14 the ratio of measured velocity to the pressure drop has been plotted against the diameter of the beads for the tests done with water. The nominal diameter of coarse tungsten carbide particles were estimated to be 0.04 mm.

A polynomial curve was fitted through the data points. The following equation was obtained relating $\bar{u}_m/\Delta p$ and bead diameter:

$$\frac{\bar{u}_m}{\Delta p} = 1.87 + 3.17\ d + 0.542\ d^2 \qquad (12)$$

where d = bead or powder diameter (mm)

$\bar{u}_m$ = measured velocity (m/s)

Δp = pressure loss (kPa)

This equation only applies to tests with water.

Finite element analysis was done using the results of the experiment. Specifically, FEM results were obtained for tungsten carbide powders of 1, 0.21 and 0.04 mm diameters for molten steel at 50, 67 and 87 kPa gauge pressures.

Tables 4 and 5 shows some results involving Tungsten Carbide and Al_2O_3 powders for the cross-sectional and axial flow models (without eddy conductivity). These results represent some of the earlier attempts at modelling penetration depths.

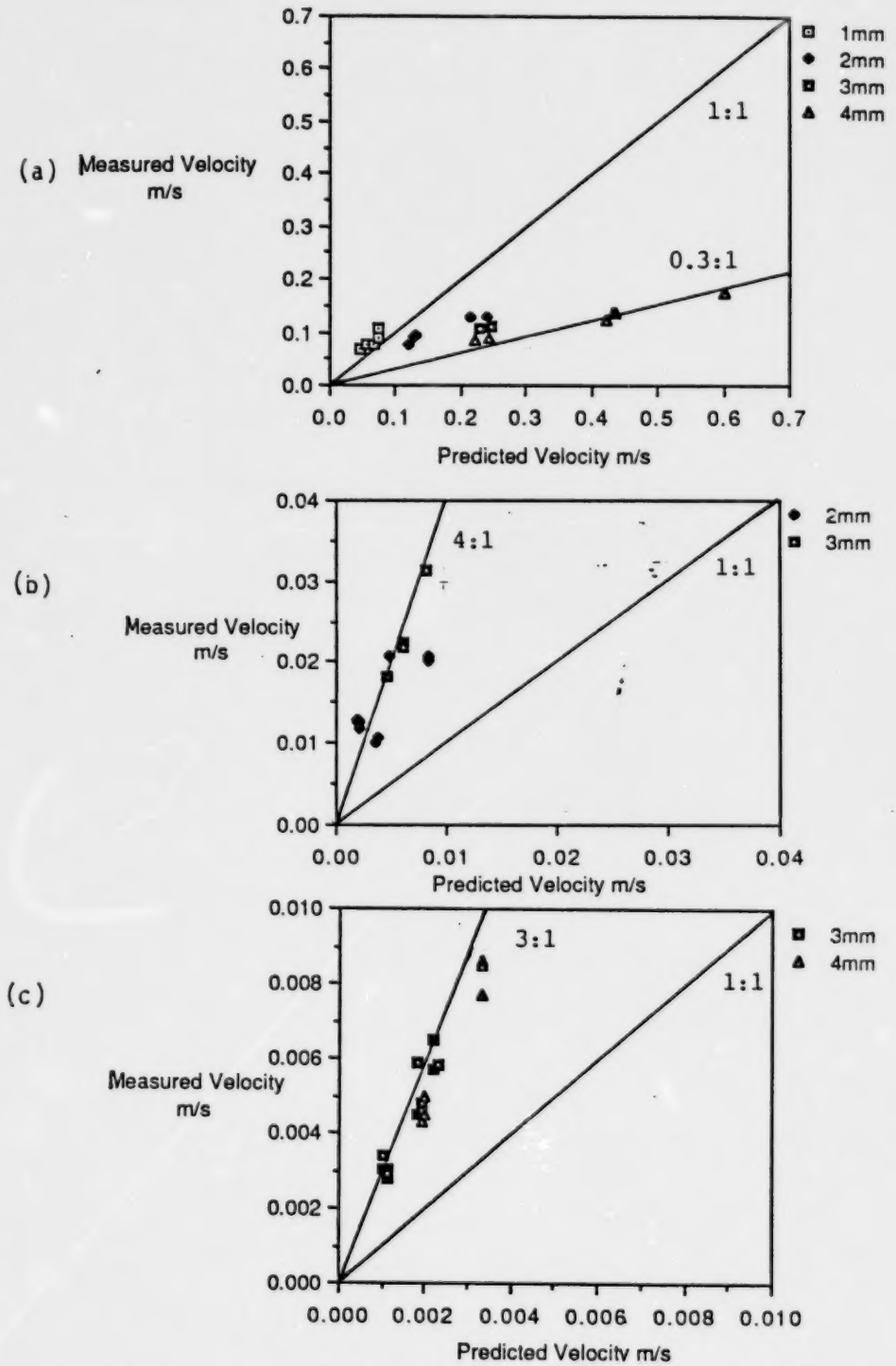

Figure 13 **Measure of Velocity Through the Glass Beads Versus Predicted Velocity, (a) in water, (b) in light oil, (c) in SAE40 oil. Note: The legends refer to nominal bead diameter.**

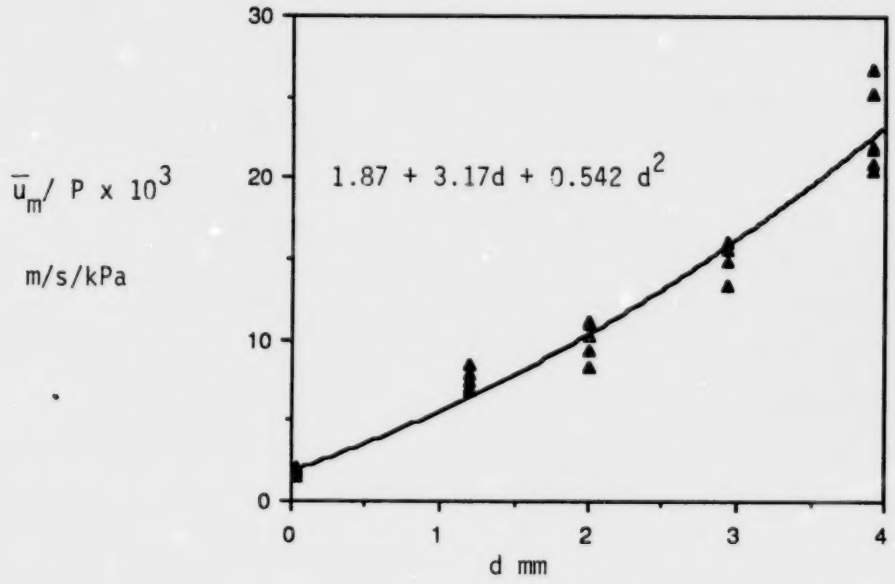

Figure 14 **Ratio of Measured Velocity to Pressure as a Function of Diameter**

TABLE 4

Results of Heat Flow Analysis

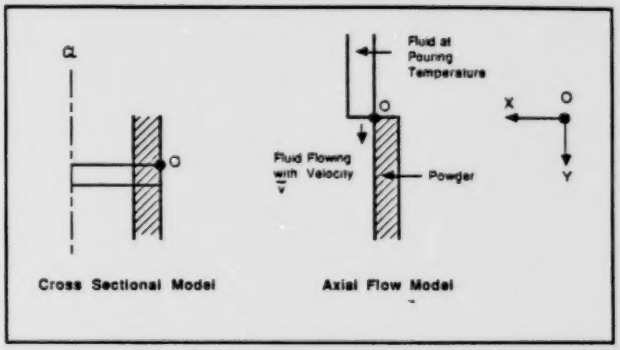

Cross Sectional Model

Powder: Al_2O_3
Nominal Diameter: 0.21mm

Time (s)	X Coordinate (mm)
0	0
.00005	.01415
.0001	.0272
.0002	.043
.0003	.06
.0004	.070

Axial Flow Model

Time (s)	X(mm)	Y(mm)
.001	.0133	0
	.0211	.21
	.0267	.43
	0	.47
.002	.0097	0
	.0143	.22
	.081	.46
	0	.51
.003	.029	0
	.041	.22
	.037	.52
	.038	.56
	0	.67
.005	.067	0
	.051	.22
	.048	.56
	.055	.83
	0	1.63

TABLE 5

Tungsten Carbide (Coarse)

Cross Sectional Model

Time (s)	X Coordinate (mm)
.00005	.0091
.0001	.018
.0002	.021
.0003	.038
.0004	.051
.0005	.063
.0006	.070

Axial Flow Model

Time (s)	X(mm)	Y(mm)
.001	.0264	0
	.0397	.1875
	.0145	.375
	0	.445
.002	.0163	0
	.0231	.1875
	.0233	.375
	0	.465
.003	.049	0
	.057	.1875
	.0385	.375
	.0356	.5625
	0	.766
.004	.0534	0
	.0650	.1875
	.051	.375
	.044	.5625
	.027	.75
	0	.8
.005	.0765	0
	.073	.1875
	.053	.375
	.050	.625
	.0283	.93
	0	1.11

Figure 15 shows the temperature distribution through the tube radius at various instances of time for metal flow through 0.35 mm diameter particles. Complete solidification is deemed to occur when centre-line temperature reached 1450°C, i.e. at 0.002253 s. For a slow speed of 33 mm/s, this corresponds to 0.074 mm of metal penetration.

Figures 16 to 18 show the plots of the interfacial temperature (i.e. at the molten metal/particle wall interface) as a function of time for the three gauge pressures of 50, 67 and 87 kPa for 0.04 mm particle size. At the instant of time, when the interfacial temperature reaches 1450°C, the solidification is assumed to start. The time multiplied by the corresponding fluid velocities (i.e. $V \cdot t$) provides us with the 'penetration due to fluid flow (i.e. P_F)'.

Figures 19 and 20 shows the main flow penetration before the start of solidification and the penetration during solidification due to various applied gauge pressures. Figure 21 is a plot of total penetration through the particle layers for three gauge pressures of 50, 67 and 87 kPa respectively. Figure 22 shows the typical eddy conductivity values used for calculation.

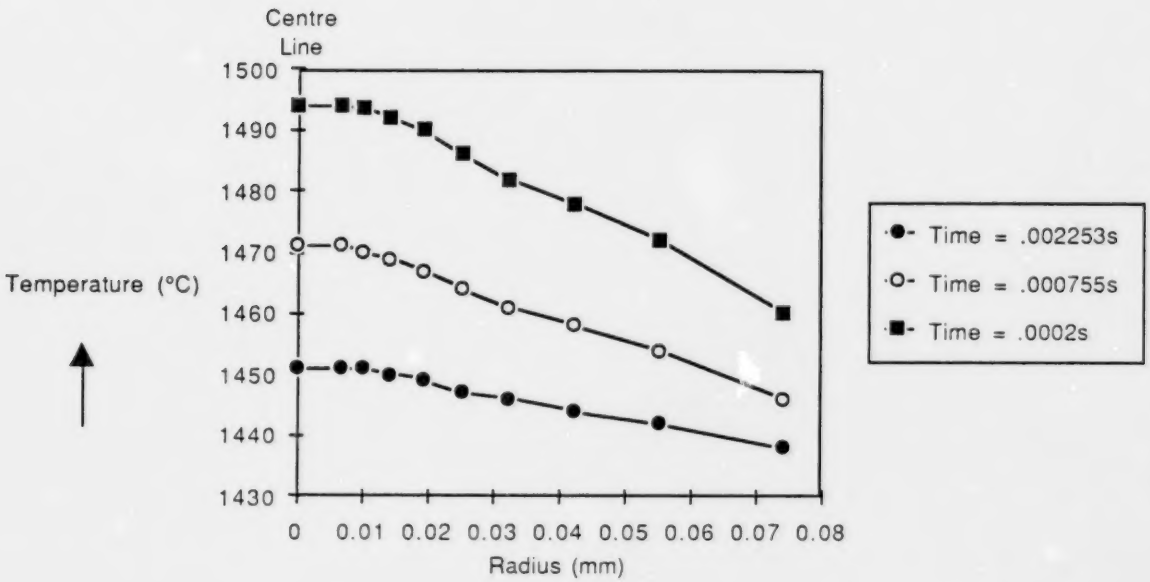

Figure 15 Penetration During Solidification for 0.35mm Particle

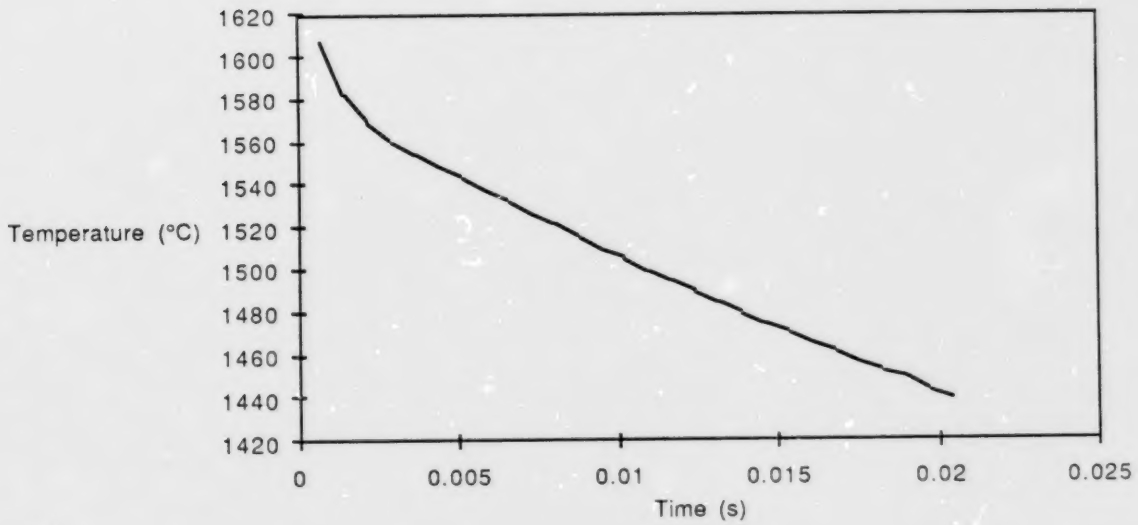

Figure 16 Interfacial Temperature for 0.04 mm Particle (Gage Pressure = 50 kPa, Velocity = 21mm/s)

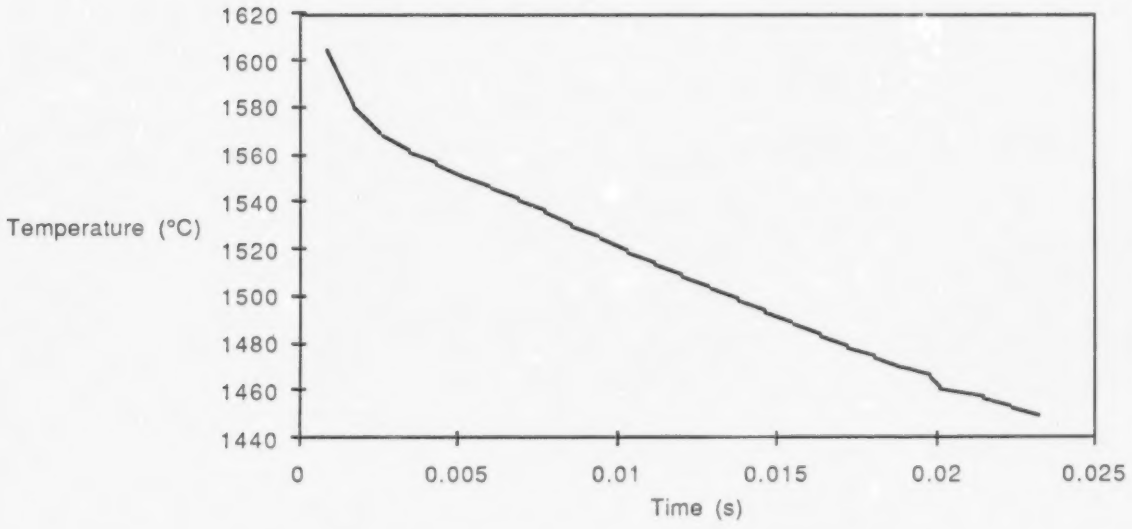

Figure 17 Interfacial Temperature for 0.04 mm Particle (Gage Pressure = 67 kPa, Velocity = 28mm/s)

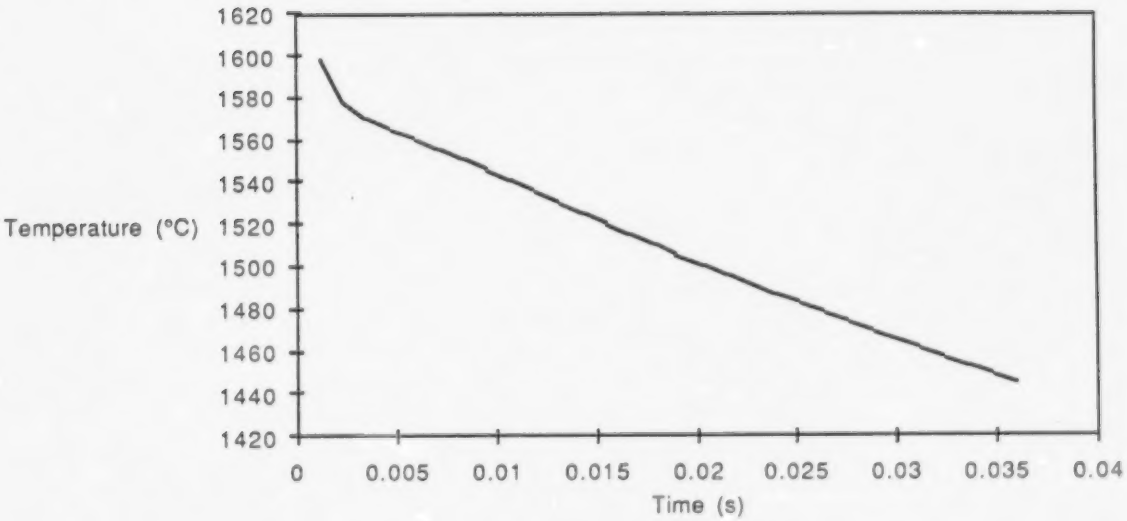

Figure 18 Interfacial Temperature for 0.04 mm Particle (Gage Pressure = 87 kPa, Velocity = 33mm/s)

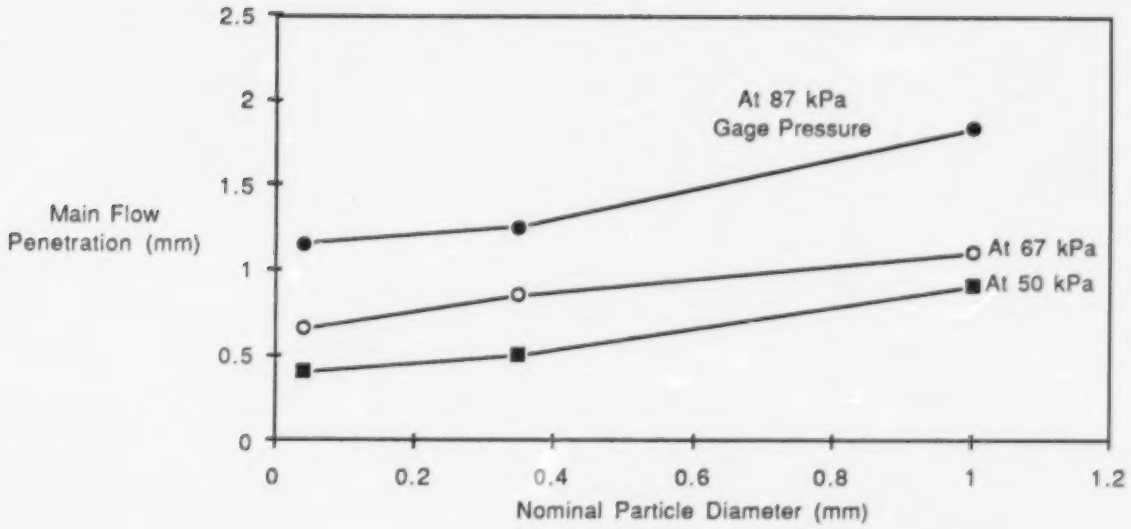

Figure 19 Main Flow Penetration as a Function of Particle Diameter and Gage Pressure

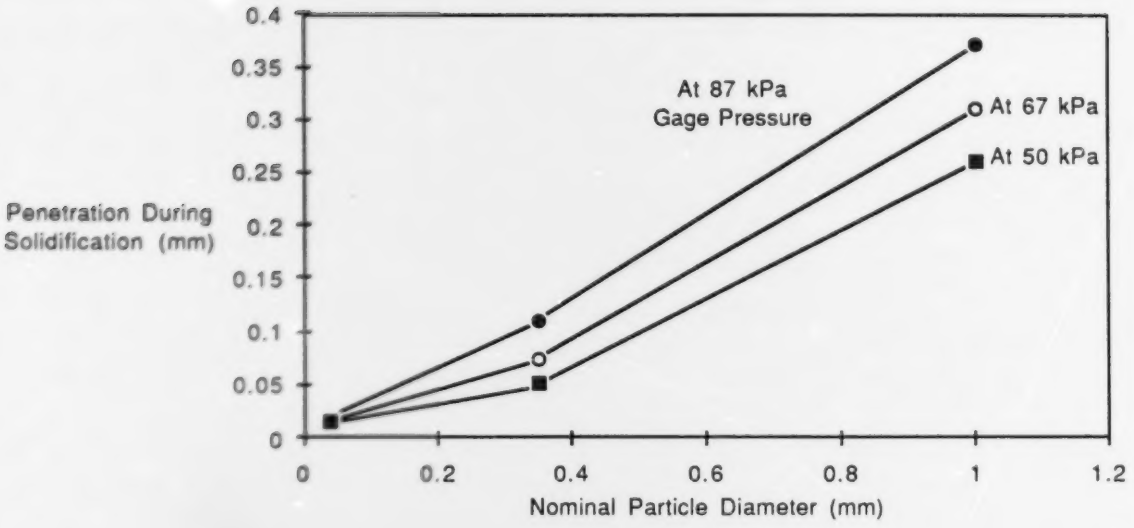

Figure 20 Penetration During Solidification as a Function of Particle Diameter and Gage Pressure

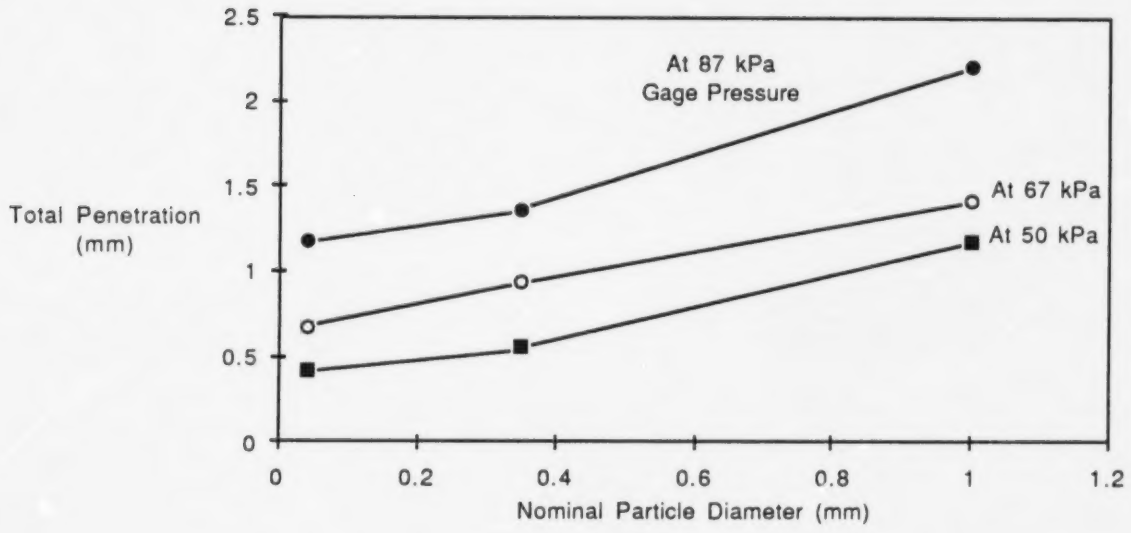

Figure 21 Total Penetration as a Function of Particle Diameter and Gage Pressure

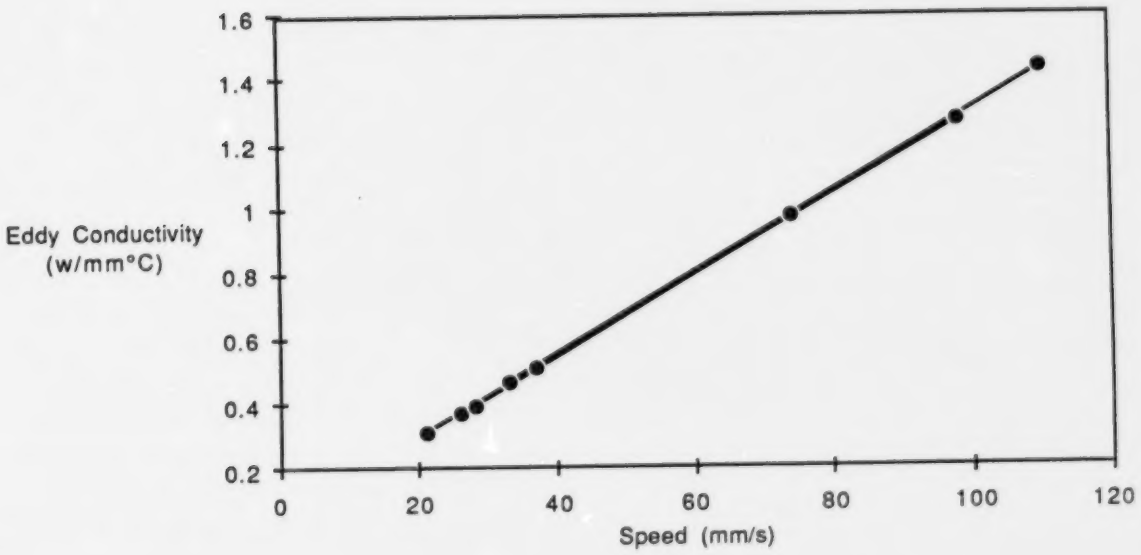

Figure 22 Eddy conductivity Values

5. DISCUSSION

The simplest analytical solution to the problem of predicting freezing time (and hence the fluid life) in a cylindrical mold at zero superheat is given by [14]

$$\tau_F = \frac{P_h}{2}\left(\frac{1}{B_i} + \frac{1}{2}\right) \qquad (13)$$

where τ_F = dimensionless freezing time ($\alpha tF/ro^2$)

P_h = latent heat ($L/C[T_M-T_A]$)

Bi = heat transfer coefficient ($\frac{hro}{K}$)

L = latent heat of fusion

C = specific heat of solidified metal

T_M = melting temperature of pure metal

T_A = ambient temperature (initial temperature of the tube)

α = thermal diffusivity of metal at T_M

t_F = fluid life and time to complete freezing

ro = internal radius of the tube

h = heat transfer coefficient

k = thermal conductivity of the solidified metal in the range T_A to T_M

This solution was originally developed for the freezing of ice. Substituting for the parameters in equation (13), we have

$$t_F = \frac{L\ ro}{2c(T_M-T_A)} \cdot \frac{1}{\alpha}\left[\frac{k}{h} + ro\right] \qquad (14)$$

Substituting the appropriate values in equation (14), we have,

$$t_F = \frac{L\ ro^2}{C\alpha(T_M-T_A)}\left[\frac{k}{hro} + \frac{1}{2}\right] \qquad (15)$$

$$= \frac{27.89}{h} + 6.64\ E\text{-}6 \qquad (16)$$

The heat transfer coefficient of 500 $W/m^2°C$ was obtained from cooling curves at the mold/metal interface for gravity injection into the 3 mm bore Pyrex mold by Pai et al [14]. Using the same values of h, viz. 500 w/m^2 in equation (16), we obtain

$$t_F = 0.0125 \text{ s}$$

Assuming that this is the time that is available for the fluid to flow, the total penetration (velocity = 21 mm/s through 0.04 mm particle tube) will be 0.26 mm for 50 kPa gauge pressure. This solution will overestimate the actual rate of freezing in other than Newtonian Conditions by assuming a linear temperature distribution in the solidified shell.

Similar calculations were done for all the cases, and are shown in Table 6. From observations at PMRL, penetration of more than a few millimeters have not been observed. So, it is possible that the value of heat transfer coefficient (500 $w/m^2°C$) assumed may be in error for the calculation of penetration shown in Table 6.

The basic hypothesis that the flow is laminar was checked. Reynold's number $Re = Vx/\nu$, where ν is the kinematic viscosity V, the mean flow velocity and x is the characteristic distance (diameter of the capillary tube, in our case). For $Re \ll 2000$, the flow was considered laminar. The calculated Reynolds' numbers are shown in Table 7.

Matsuda et al [7] conducted research regarding the heat transfer and fluidity of flowing metal in cylindrical mold cavities. He concluded that the temperature distribution can be obtained through equations of the form:

$$\theta_F - \theta_I = \left[\frac{M}{\sqrt{t - t_2}} + \frac{M'}{ro} \right] \frac{t_2}{\rho c \; ro} \qquad (17)$$

where M = Mold constant

M' = Cylindrical mold constant

t = Flow time of leading tip

t_2 = Flow time from entrance

ro = Radius of mold channel

ρc = Volumetric specific heat

In the above equation, the radius of the capillary tube is in the denominator. As 'ro' approaches zero, the temperature goes to infinity. No limits were placed in the derivation of equation (17).

TABLE 6

CALCULATIONS BASED ON EQUATION (14)

Nominal Particle Diameter (mm)	Equivalent Capillary Diameter (mm)	Gauge Pressure (kPa)	Velocity (mm/s)	Time to Freeze (s)	Penetration (mm)
.04	.02	50	21	.0125	.26
.35	.15	50	26	.10	2.6
1.00	.44	50	73.8	.30	22.14
.04	.02	67	28	.0125	0.35
.35	.15	67	33	.1	3.30
1.00	.44	67	97.8	.3	29.34
.04	.02	87	33	.0125	0.41
.35	.15	87	37	.1	3.70
1.00	.44	87	110	.3	33

TABLE 7

CALCULATION OF REYNOLD'S NUMBER

Mean Velocity (mm/s)	Capillary Diameter (mm)	Reynolds' Number
21	.02	.44
26	.15	4.06
73.8	.44	33.8
28	.02	0.58
33	.15	5.15
97.8	.44	44.78
33	.02	0.69
37	.15	5.77
110	.44	50.36

Kinematic Viscosity = 0.961×10^{-6} m^2/s assumed.

In our case, an attempt was made to use equation (17). However, since in all the cases radii of the tube were small, the above equation gave erroneous results.

Results of total penetration (Figure 21) indicate that increasing the gauge pressure (and hence velocity of flow) increases the penetration through the particle wall. Also, Figure 23 shows the relationship between the flow velocity and total penetration. These curves show only small departures from linearity, which indicates a nearly uniform velocity of flow from entry to cessation of flow. Figure 23 also shows that increasing the capillary diameter (hence particle size) increases the total penetration. This observation is consistent with the results obtained by Pai et al [14] in their study of fluidity of liquid tin through Pyrex tube molds.

During the beginning of this project, it was thought that the 'cross-sectional' model would give acceptable results. During analysis it was obvious that the molten metal was losing heat much faster to the particle wall due to the large temperature gradients and also because of the fact that the effective heat flow area of the particles were larger than the cross sectional area of the molten metal. As a result, the molten metal in contact with the mold was freezing in micro seconds, suggesting very small penetration. Also, in reality, there will be oxide layers, etc., which will affect heat flow path by changing the contact resistance. The contact at the interface is also not continuous. Moreover, due to the tortuiosity of the channels, the fluid flow undergoes change in direction, and local velocities might be quite different than the average mean velocity assumed in this study. The individual paths are interconnected in a complex way and there may be numerous abrupt changes in cross-section at which additional pressure drops can occur. Also, as the flow paths are not straight there are accelerations and inertia forces which do not arise in flow through straight capillary tubes.

In the present study, another important factor that has not been considered is the dissolution kinetics. Tungsten carbide does not dissolve to a great extent in molten steel. However, WC powders used at PMRL contain about 6% Cobalt, which is highly soluble in steel. In the presence of dissolution, the capillary tube diameter will increase with time and hence penetration is expected to be greater. The present model can be readily modified to consider dissolution aspects.

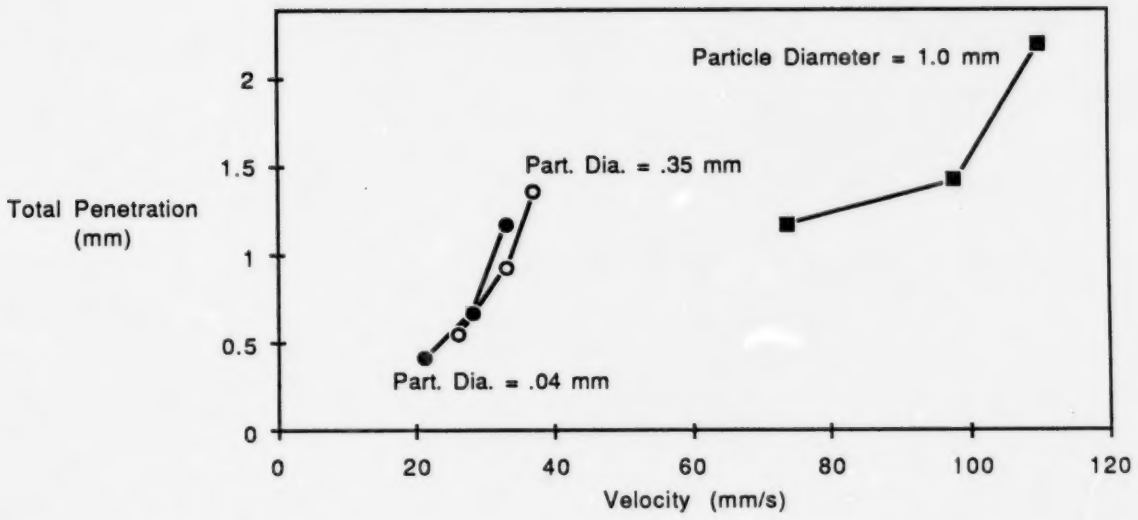

Figure 23 Total Penetration as a Function of Flow Velocity

6. CONCLUSIONS

The following conclusions can be drawn from the present study:

1. The results of total penetration indicate that increasing gauge pressure increases the penetration through the particle wall.

2. The relationship of total penetration and flow velocity show only small departures from linearity, which indicates a nearly uniform velocity of flow from entry to cessation of flow.

3. The penetration appears to be more or less independent of particle diameter. This observation is consistent with PMRL conclusions. The maximum penetration observed is about 2 mm for 1 mm diameter particle. However, in practice, the penetration observed at PMRL is 3 to 4 mm. Thus, the model predicts a lower penetration depth. This could be attributed to various assumptions made in the model.

4. Fluid flow dominates the phenomena. It will be necessary to solve the coupled Navier-Stokes, continuity and energy equations with "strong" free surface effects. A modified version of the 'SOLA' code would be appropriate.

5. After the fluid flow effects are explored, then the issue of dissolution of particles could be examined.

REFERENCES

[1] Davis, K.G., Magny, J.G., "Cast-in-place Hardfacing", Physical Metallurgy Research Laboratories Report No. PMRL 80-90 (J).

[2] Fand, R.M., Kim, B.Y.K., Lam, A.C.C. and Phan, R.T., "Resistance to the Flow of Fluids Through Simple and Complex Porous Media Whose Matrices are Composed of Randomly Packed Spheres", Trans. ASME, Vol. 109, Sept. 1987, pp. 268.

[3] Irmay, S., "On the Theoretical Derivation of Darcy and Forchheimar Formula", Trans. Am. Geo. Union, Vol. 39, No. 4, 1958, pp 702.

[4] Palewal, M., Apelian, D. and Langford, G., "Performance of a Porous Refractory Value for Liquid Metals", Met. Trans. B, Volume IIB, March 1980, pp 39.

[5] Kolling, M. and Grigull, V. "Heat and Mass Transfer in Metallurgical Systems" ed. Spalding, D.B. and Afgan, H.H., pp. 329, 1981, Washington, D.C., Hemisphere Publishing Co.

[6] Pai, B.C. and Jones, H. "Solidification Technology in the Foundary and Casthouse, pp 126, 1983, London. The Metals Society.

[7] Matsuda, M. and Ohmi, M. "Heat Transfer Analysis and Fluidity of Flowing Metal in a Cylindrical Mold Cavity", AFS International Cast Metals Journal", December 1981, pp 18.

[8] Davies, V. de L. "Feeding Range Determination by Numerically Computed Heat Distribution", AFS Cast Metals Research Journal, June 1975, pp 33.

[9] Murr, L.E., "Interfacial Phenomena in Metals and Alloys", pp 87, Addison Wesley Publishing Co, MA, 1975.

[10] Argyropoulos, S.A. and Guthrie, R.I.L. "Dissolution Kinetics of Ferro Alloys in Steelmaking", pp 156.

[11] Thomas, B.G., Samarasekera, I.V. and Brimacombe, J.K. "Mathematical Model of the Thermal Processing of Steel Ingots: Part 1. Heat Flow Model", Met. Trans. B., Volume 18B, March 1987, pp 119.

[12] Harlow, F.H., "Numerical Methods for Fluid dynamics - An Annotated Bibliography", Los Alamos Scientific Laboratory Reprot, LA - 4281 (December 1969).

[13] Hist, C.W., Nichols, B.D. and Romero, N.C., "SOLA-A Numerical Solution Algorithm for Transient Fluid Flows".

[14] Pai, B.C. and 'Jones, H.' "Effect of Experimental Variables on Casting Fluidity and Fluid Life of Liquid TIN", Materials Science and Technology, May 1985, Vol. 1, pp 398.

APPENDIX A

PREDICTION OF VELOCITY AND TEMPERATURE FIELDS FOR CONFINED FLUID FLOWS

IRAP-H REPORT NO. 7-4499-H-15

PREDICTION OF VELOCITY AND TEMPERATURE FIELDS FOR CONFINED FLUID FLOWS

RESEARCH CONDUCTED AT: ARCTEC CANADA LIMITED
311 Legget Drive,
Kanata, Ontario.
K2K 1Z8

DATE: October 1987

AUTHOR: Khalid M. Chaudhury

TABLE OF CONTENTS

1. INTRODUCTION.....1

2. BASIC SOLUTION ALGORITHM.....2

2.1 Equations of Motion.....2
2.2 Finite Difference Procedure.....3
2.3 Boundary Conditions.....10

3. MODIFICATIONS FOR INCORPORATION OF HEAT TRANSPORT.....12

4. STEPS IN ONE CALCULATION CYCLE.....14

5. NUMERICAL STABILITY CONSIDERATIONS.....15

6. TEST PROBLEMS.....16

7. DISCUSSION ON RESULTS OF TEST PROBLEMS.....17

ABSTRACT

A modified version of the already existing computer program SOLA (A numerical solution algorithm for transient fluid flows), to transport heat is presented.

The modified code can be used for predicting temperature and velocity fields for confined fluid flows with Prandtl number of the order of unity (Prandtl number <<1 cause numerical instabilities in the result).

The usefulness of the modified program is shown by the solution of test problems which require calculation of transient velocity and temperature fields. The finite difference results agree with results obtained from other techniques.

1. INTRODUCTION

Numerical techniques have been used to solve time-dependent incompressible fluid flow problems for quite some time. One of the best known techniques, the Marker-and-Cell (MAC) method uses an Eulerian finite-difference formulation with pressure and velocity as the primary dependent variables. This method, originally developed specifically for problems involving free surfaces, is equally capable of treating flows in confined regions. SOLA is in fact a highly simplified MAC code. It is designed for persons with little or no experience in numerical fluid dynamics. The basic solution technique is in fact a two dimensional solution of Navier-Stokes equations in plane or axisymmetric coordinates for various boundary conditions such as:

- rigid walls with free-slip or no slip tangential velocities,
- specified inflow or outflow boundaries,
- continuative outflow boundaries and
- periodic boundaries.

The basic solution algorithm contained in the code also serves as a good foundation for developing new codes with other capabilities. For example, a scalar transport equation for density or temperature can be easily added to investigate buoyancy-driven flows and flows of stratified fluids. With some modifications of the basic equations, the SOLA solution algorithm has been adapted to saturated or unsaturated flow in porous media, to three-dimensional shallow water motions, to a drift flux approximation for two-phase flow and to almost three-dimensional flow of air or water over variable terrain for pollution dispersal models.

Although the basic code can be adopted for a wide range of applications, we will restrict ourself only to the incorporation of heat transport into the MAC technique for the present.

2. BASIC SOLUTION ALGORITHM

The following solution algorithm is for confined flows of incompressible fluids without free surfaces. (An extension of code can be made to permit the use of a free surface or curved rigid boundary, free slip, to be located across the top or bottom of the fluid region).

2.1 Equations of Motion

The differential equations to be solved are written in terms of Cartesian Coordinates (x,y). For cylindrical (axisymmetric) coordinates, x is the radial coordinate, y the axial coordinate and several additional terms must be added to the basic equations. A coefficient ζ is added to the following equations whose numerical values of either 0 or 1 corresponds to the use of plane or cylindrical geometry.

The mass continuity equation is:

$$\frac{\partial u}{\partial x} + \frac{\partial v}{\partial y} + \zeta \frac{u}{x} = 0 \qquad (1)$$

The equations of motion are the Navier-Stokes equations.

$$\frac{\partial u}{\partial t} + \frac{\partial u^2}{\partial x} + \frac{\partial uv}{\partial y} + \zeta \frac{u^2}{x} = -\frac{\partial P}{\partial x} + g_x + \nu \left[\frac{\partial^2 u}{\partial x^2} + \frac{\partial^2 u}{\partial y^2} + \zeta \left(\frac{1}{x}\frac{\partial u}{\partial x} - \frac{u}{x^2} \right) \right]$$

$$\frac{\partial v}{\partial t} + \frac{\partial uv}{\partial x} + \frac{\partial v^2}{\partial y} + \zeta \frac{uv}{x} = -\frac{\partial P}{\partial y} + g_y + \nu \left[\frac{\partial^2 v}{\partial x^2} + \frac{\partial^2 v}{\partial y^2} + \frac{\zeta}{x}\frac{\partial v}{\partial x} \right] \qquad (2)$$

The velocity components (U,V) are in the coordinate directions (x, y), P is the ratio of pressure to constant density, and (g_x, g_y are body forces due to gravity. The kinematic viscosity coefficient is denoted by the constant ν.

2.2 Finite Difference Procedure

The finite difference mesh used for numerically solving the above equations consists of rectangular cells of width δx and height δy. The mesh region containing fluid is composed of IBAR cells in X-direction labelled with index i, and JBAR cells in the Y-direction, labelled with index j. The fluid region is surrounded by a single layer of fictitious cells so that the cells in the complete mesh total IMAX = IBAR +2 by JMAX = JBAR +2 (See Figure 1).

Fluid velocities and pressures are located at all positions as shown in Figure 2.

Where U is the velocity at the middle of the vertical sides of a cell and V is the velocity at the middle of the horizontal sides of the cell, and P is the pressure at the cell center.

The finite difference notation used in this report is:

$P^n_{i,jn}$ = Pressure at center of cell (i,j) at time level n

$T^n_{i,j}$ = Temperature at center of cell (i,j) at time level n

$U^n_{i,j}$ = X-direction velocity at middle of right side of cell (i,j) at time level n

$V^n_{i,j}$ = Y-direction velocity at middle of top side of cell (i,j) at time level n

Subscripts are used for all locations and superscripts are used for the time level at which the quantities are evaluated such that $t = n*\delta t$, where δt is the time increment.

The difference approximation representing the continuity equation, Equation (1), for a typical cell (i,j) is:

$$\frac{1}{\delta x}\left(U^{n+1}_{i,j} - U^{n+1}_{i-1,j}\right) + \frac{1}{\delta y}\left(V^{n+1}_{i,j} - V^{n+1}_{i,j-1}\right)$$

$$+ \frac{\xi}{2\delta_x(i-1.5)}\left(U^{n+1}_{i,j} + U^{n+1}_{i-1,j}\right) = 0 \qquad (3)$$

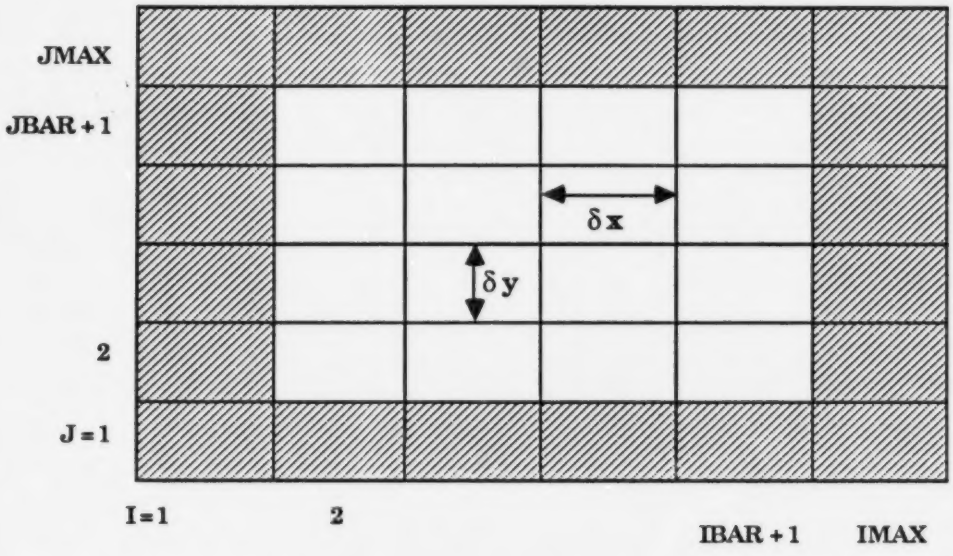

Figure 1 **GENERAL MESH ARRANGEMENT.**
(fictitious boundary cells are shaded)

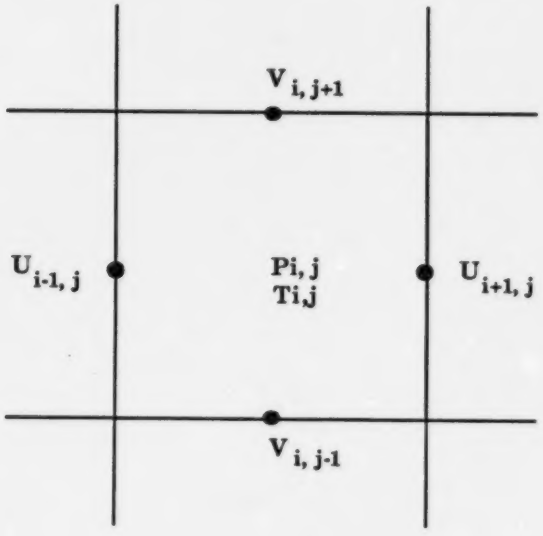

Figure 2 **ARRANGEMENT OF FINITE DIFFERENCE VARIABLES IN A TYPICAL CELL**

Similarly the difference equations approximating the Navier-Stokes equations, Equation (2), are:

$$u_{i,j}^{n+1} = u_{i,j}^{n} + \delta t \left[\frac{1}{\delta x} \left(P_{i,j}^{n} - P_{i+1,j}^{n} \right) + g_x - FUX - FUY - FUC + VISX \right] \quad \text{and}$$

$$v_{i,j}^{n+1} - v_{i,j}^{n} + \delta t \left[\frac{1}{\delta y} \left(P_{i,j}^{n} - P_{i,j+1}^{n} \right) + g_y - FVX - FVY - FVC + VISY \right] \qquad (4)$$

Where the convective and viscous fluxes are defined as:

$$FUX = \frac{1}{4\delta x} \left[\left(u_{i,j} + u_{i+1,j} \right)^2 + \alpha | u_{i,j} + u_{i+1,j} | \cdot \left(u_{i,j} - u_{i+1,j} \right) - \left(u_{i-1,j} + u_{i,j} \right)^2 - \alpha | u_{i-1,j} + u_{i,j} | \left(u_{i-1,j} - u_{i,j} \right) \right] ,$$

$$FUY = \frac{1}{4\delta y} \left[\left(v_{i,j} + v_{i+1,j} \right) \left(u_{i,j} + u_{i,j+1} \right) + \alpha | v_{i,j} + v_{i+1,j} | \left(u_{i,j} - u_{i,j+1} \right) - \left(v_{i,j-1} + v_{i+1,j}{}^{-1} | \left(u_{i,j-1} + u_{i,j} \right) - \alpha | v_{i,j-1} + v_{i+1,j-1} | \left(u_{i,j-1} - u_{i,j} \right) \right] ,$$

$$FUC = \frac{\xi}{8\delta x(i-1)} \left[\left(u_{i,j} + u_{i+1,j}\right)^2 + \left(u_{i-1,j} + u_{i,j}\right)^2 \right.$$

$$+ \alpha|u_{i,j} + u_{i+1,j}|\left(u_{i,j} - u_{i+1,j}\right)$$

$$\left. + \alpha|u_{i-1,j} + u_{i,j}|\left(u_{i-1,j} - u_{i,j}\right)\right] \quad ,$$

$$FVX = \frac{1}{4\delta y} \left[\left(u_{i,j} + u_{i,j+1}\right) \left(v_{i,j} + v_{i+1,j}\right) \right.$$

$$+ \alpha|u_{i,j} + u_{i,j+1}| \left(v_{i,j} - v_{i+j,1}\right)$$

$$- \left(u_{i-1,j} + u_{i-1,j+1} \left(v_{i-1,j} + v_{i,j}\right)\right.$$

$$\left. - \alpha|u_{i-1,j} + u_{i-1,j+1}|\left(v_{i-1,j} - v_{i,j}\right)\right] \quad ,$$

$$FVY = \frac{1}{4\delta y} \left[\left(v_{i,j} + v_{i,j+1}\right)^2 \alpha|v_{i,j} + v_{i,j+1}| \cdot \right.$$

$$- \left(v_{i,j} - + v_{i,j+1}\right) - \left(v_{i,j-1} + v_{i,j}\right)^2$$

$$\left. - \alpha|v_{i,j-1} + v_{i,j}| \quad \left(v_{i,j-1} - v_{i,j}\right)\right] \quad ,$$

$$FVC = \frac{\xi}{8\delta x(i-1.5)} \left[\left(u_{i,j} + u_{i,j+1}\right) \left(v_{i,j} + v_{i+1,j}\right) \right.$$

$$+ \left(u_{i-1} + u_{i-1,j+1}\right) \left(v_{i-1,j} + v_{i,j}\right)$$

$$+ \alpha|u_{i,j} + u_{i,j+1}| \left(v_{i,j} - v_{i+1,j}\right)$$

$$\left. + \alpha|u_{i-1,j} + u_{i-1,j+1}| \left(v_{i-1,j} - v_{i,j}\right)\right] \quad ,$$

$$VISX = \nu \left[\frac{1}{\delta x^2} \left(v_{i+1,j} - 2u_{i,j} + u_{i-1,j}\right) \right.$$

$$+ \frac{1}{\delta y^2} \left(u_{i,j+1} - 2u_{i,j} + u_{i,j-1}\right)$$

$$\left. + \frac{\xi}{2\delta x^2(i-1)} \left(u_{i+1,j} - u_{i-1,j}\right) - \frac{\xi u_{i,j}}{\delta x^2(i-1)^2} \right] \quad ,$$

and

$$VISY = \nu \left[\frac{1}{\delta x^2} \left(v_{i+1,j} - 2v_{i,j} + v_{i-1,j}\right) \right.$$

$$+ \frac{1}{\delta y^2} \left(v_{i,j+1} - 2v_{i,j} + v_{i,j-1}\right)$$

$$\left. + \frac{\xi}{2\delta x^2(i-1.5)} \left(v_{i+1,j} - v_{i-1,j}\right) \right] \quad . \qquad (5)$$

..

All quantities in the above convective and viscous fluxes are to be evaluated at time $n\delta t$. The coefficient α in the above equations gives the desired amount of upstream differencing; that is, when $\alpha = 0$, these equations are centered in space and are numerically unstable and generally requires some viscosity ν to remain stable. In general α should be chosen slightly larger than the maximum value of

$$\left| \frac{u\delta t}{\delta x} \right| \quad \text{or} \quad \left| \frac{v\delta t}{\delta y} \right|$$

occurring in the mesh.

The velocities computed according to Equations (4) will not, in general, satisfy the continuity equation, Equation (3). This incompressibility constraint is imposed by adjusting the cell pressures (done interatively). The pressure change δp required to make the divergence (D) of cell equal to zero is given by:

$$\delta P = -D / \left[2\delta t \left(\frac{1}{\delta x^2} + \frac{1}{\delta y^2} \right) \right]$$

the new cell pressure is then $P_{i,j} + \delta p$ and the velocity components at the sides of the cell are adjusted to reflect this change.

In some cases, convergence of the interaction can be accelerated by multiplying δp with an over-relaxation factor w. A value of 1.8 for w is optimum but a larger value will result in unstable iteration.

2.3 Boundary Conditions

The boundary conditions can be imposed by setting appropriate velocities (also temperatures, in the case of heat transport) in the fictitious cells surrounding the mesh. Following are different kinds of boundary conditions which are used routinely.

1. Rigid free-slip wall
2. Rigid no slip wall
3. Continuative outflow wall
4. Periodic wall in X or Y direction

In this report, we deal specifically with the first two of the above boundary conditions. Consider, for example, the left boundary of the computing mesh. If this boundary is to be a rigid free-slip wall, the normal velocity here must be zero and the tangential velocity, should have no normal gradient, i.e.,

$$\left.\begin{aligned} U_{1,j} &= 0 \\ V_{1,j} &= V_{2,j} \end{aligned}\right\} \text{for all } j.$$

Similarly if the left wall is a no-slip rigid wall, then the conditions imposed are given as:

$$\left.\begin{aligned} V_{1,j} &= 0 \\ V_{1,j} &= -V_{2,j} \end{aligned}\right\} \text{for all } j.$$

These conditions are imposed on the velocities resulting from the Equation 4 and are imposed after each pass through the mesh during pressure iteration. Boundary conditions similar to these for the left wall are used at the right, top and bottom boundaries of the mesh as well.

To increase the usefulness of the basic code, specified inflow and outflow boundaries and obstacles inserted within fluid region are desirable. This can be achieved by prescribing additional velocities or temperatures to existing boundary conditions. A place has been reserved for the addition of special boundary conditions at the end of main boundary condition section in the computer programs (See Flow Chart).

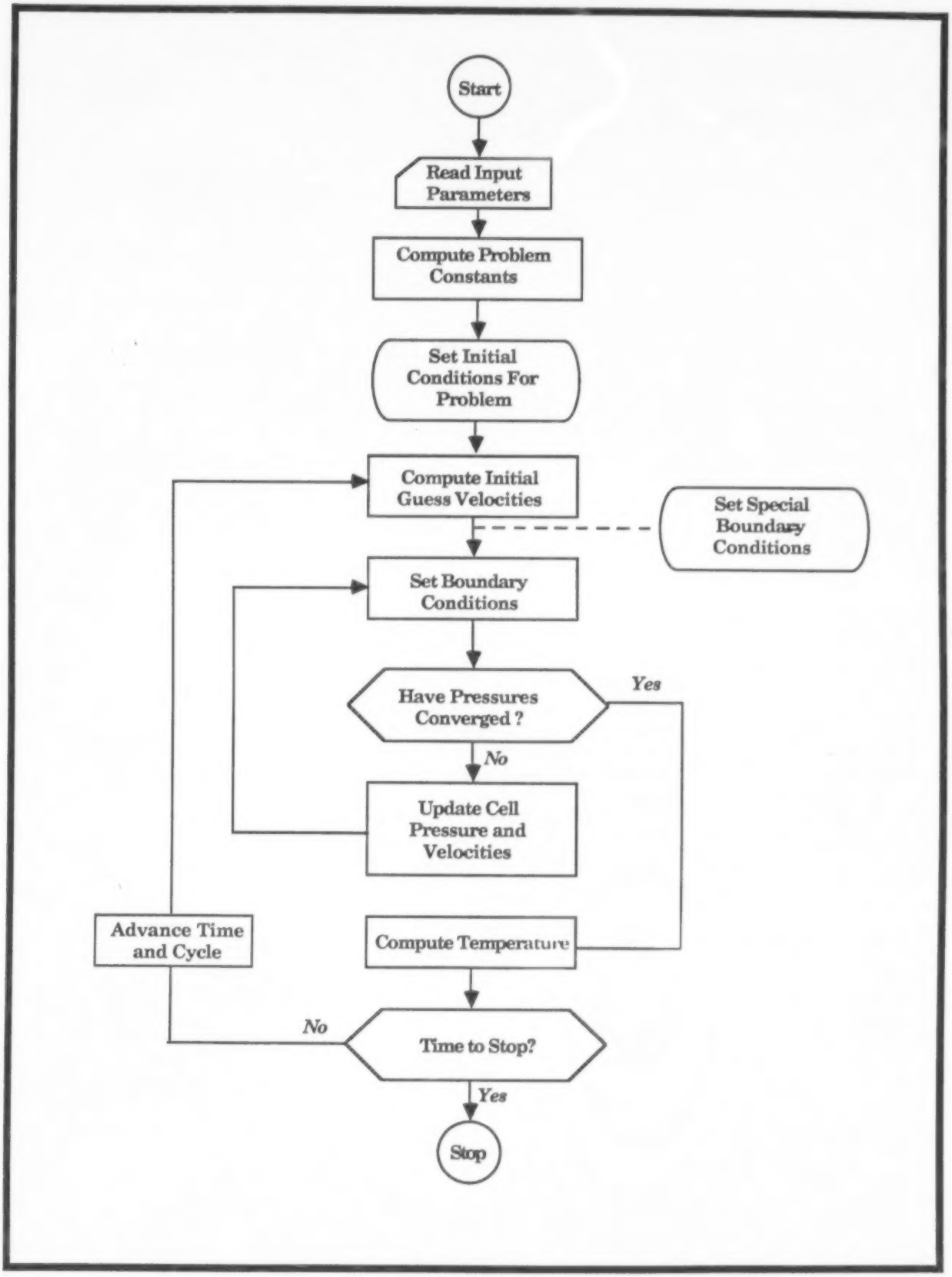
Start
Read Input Parameters
Compute Problem Constants
Set Initial Conditions For Problem
Compute Initial Guess Velocities
Set Special Boundary Conditions
Set Boundary Conditions
Have Pressures Converged ?
Yes
No
Update Cell Pressure and Velocities
Advance Time and Cycle
Compute Temperature
No
Time to Stop?
Yes
Stop

3. MODIFICATIONS FOR INCORPORATION OF HEAT TRANSPORT

The dynamics of the incompressible flows are essentially unaffected by the distribution of heat, so that the latter simply accommodates itself to the changes in the fluid configuration. This simple uncoupling is by no means a universal property of "incompressible" flows, however. The most common exception arises from variations of viscosity with temperature. Buoyancy effects may also be an important manifestation of temperature variations. The incorporation of heat transport into the MAC calculations is quite a straight forward process. It is necessary only to add a step to the sequence of processes that advance all field variables each cycle.

Even if the heat flow effects couple back to the dynamics, the required modifications are relatively simple to include. (Not tackled in this report.)

The basic equation for heat transport can be specialized directly from the general energy equation of fluid dynamics.

$$\frac{\partial I}{\partial t} = - \rho \vec{u} . \nabla I - p \nabla . \vec{u} + \nabla . K \nabla T + \rho \nu \Phi \qquad (6)$$

where I is the internal (heat) energy per unit mass, often expressed as a product of specific heat and temperature; T is the temperature; K is the heat conduction coefficient; and Φ is proportional to the rate of heat production caused by viscous dissipation.

The first term on the right hand side of the above equation represents the convection of heat produced by fluid motion. The second term is the heat production rate from compressive effects. It ignored for incompressible flows. The third term gives heat flow from conduction processes and finally the last term is negligible for incompressible flows.

Thus for most purposes, it is sufficient to write for heat transport:

$$\frac{\partial T}{\partial t} = -V . (\vec{uT}) + \frac{\nu}{Pr} \nabla^2 T \qquad (7)$$

here Pr is the Prandtl number.

The above equation can be written in the form of a difference equation as follows:

$$T^{n+1}_{i,j} = T^{n}_{i,j} + \delta t \left[\frac{1}{\delta x} \left[(UT)^{n}_{i-1,j} - (UT)^{n}_{i+1,j} \right] + \frac{}{} \left[(VT)^{n}_{i,j-1} - (VT)^{n}_{i,j+1} \right] \right]$$

$$+ \frac{\nu}{Pr} \left[\frac{1}{\delta x^2} \left(T^{n}_{i+1,j} + T^{n}_{i-1,j} - 2T^{n}_{i,j} \right) + \frac{1}{\delta y^2} \left(T^{n}_{i,j+1} - T^{n}_{i,j-1} - 2T^{n}_{i,j} \right) \right] \right] \quad (8)$$

Appropriate boundary conditions for the heat equation can be derived directly from the physical requirements of insulation or constant temperature at a wall.

4. STEPS IN ONE CALCULATION CYCLE

The major steps involved in completing one calculation cycle are:

1. Computation of guesses for the new velocities for the entire mesh from Equation (4), which involves only the previous time values for the contributing pressures and velocities in the various flux contributions.

2. Adjustment of velocities interatively to satisfy the continuity equation, Equation (3), by making appropriate changes in the cell pressures. In the iteration, each cell is considered successively and is given a pressure change that drives its instantaneous velocity divergence to zero.

3. Finally, when convergence has been achieved, the horizontal and vertical velocities are used to calculate temperatures for the entire mesh. In the very first cycle the initial temperature of the fluid serves as temperature in the previous time step.

4. In this step the calculated velocity, pressure, temperature fields are at the advanced time level and if required, these may be used as starting values to be used in the next cycle.

5. NUMERICAL STABILITY CONSIDERATIONS

The computed quantities in numerical calculations often develop large, high frequency oscillations in time, space or both. This behaviour is referred to as numerical instability. In case of physical problems with unstable solutions, if the calculated results exhibit significant variations over distances comparable to a cell width or over times comparable to time increment, the accuracy of results can not be relied on. Hence certain restrictions must be observed in defining the mesh increments δx and δy, the time increment δt, and other factors such as α (the upstream differencing parameter).

For accuracy of results, the mesh increments must be chosen small enough to resolve the expected spatial variations in all dependent variables.

The choice of time increment necessary for stability is governed by two restrictions, namely:

1. Material can not move through more than one cell in one time step, because the difference equations assume fluxes between adjacent cells. This requires that:

$$\delta t < \min \left\{ \frac{\delta x}{|u|} , \frac{\delta y}{|V|} \right\}$$

2. For the case of non zero value of kinematic viscosity, momentum must not diffuse more than one cell diameter. This requires that:

$$\nu \delta t < \frac{1}{2} * \frac{\delta x^2 \ \delta y^2}{\delta x^2 + \delta y^2}$$

and lastly, for α, as already mentioned before, the following relation should hold:

$$1 \geq \alpha > \max \left\{ \left| \frac{u \delta t}{\delta x} \right| , \left| \frac{v \delta t}{\delta y} \right| \right\}$$

6. TEST PROBLEMS

The effectiveness of a computer program is established by the satisfactory solution of the test problems. The test problems are selected in such a way as to expose the major functions of the program. It is always necessary to have either analytical solutions or solutions by any other means so that it can be compared with the results obtained from the new computer program. Only then a decision can be made regarding the proper working of the modified program.

The following two problems were selected on the basis of the above criteria and were solved by the new finite difference program. A brief description of each problem is given below:

Problem 1: To compute the flow generated in a viscous fluid in a square cavity when the top boundary of the cavity is impulsively set into motion parallel to itself. The fluid is given an initial temperature of unity and the walls are not insulated so as the heat can flow in both x and y direction. The obtained velocity and temperature fields are discussed in the next section.

Problem 2: Fluid in a capillary tube, 0.15 cm wide and 1.95 cm deep, is initially at rest and is heated constantly from outside by a heat source. Initial temperature of the fluid is 20°C and the heat source is at 1200°C. The time required to reach a steady state is calculated by finite difference methods and is compared with the results obtained from ASGARD heat transfer analysis program. The comparison is given in the following section.

7. DISCUSSION ON RESULTS OF TEST PROBLEMS

(a) The first sample problem uses a 5 x 5 mesh, i.e., IBAR = JBAR = 5. All the boundaries are no slip walls. The fluid is initially at rest and the sliding of top boundary conditions is imposed by using a special boundary condition, i.e.,

$$U_{i,j_{max}} = 1.0 \text{ for } i = 1, I_{max}$$

The fluid is initially at a temperature of unity and the heat is allowed to conduct through the walls. We see from the results that in the initial cycles, the cell adjacent to left and right walls of the cavity begin to lose temperature. The vertical and horizontal velocities indicate that flow adjacent to upper and bottom walls has no vertical velocity component. The bulk of the fluid shows the tendency of circulatory flow. This is confirmed by the velocity plot. It was found that a steady state in velocity was reached only after 0.2 seconds. We know the temperature in the advanced time level depends directly on the temperature in the previous time and vertical and horizontal velocities. So the regions of the mesh which do not exhibit any significant change in the vertical and horizontal velocities will have smaller temperature change. The temperature drops gradually until the velocities reach a steady state, afterwards the decrease is ever so slow but theoretically they should drop and reach a steady state with the outside temperature after a sufficiently long time.

The results obtained from the modified program were compared with an already existing solution and a good agreement was seen for velocity fields. The obtained temperature fields seem reasonable too.

b) In the second problem a 3 x 12 mesh was used. The fluid is initially at rest and is at 20°C. The capillary tube is constantly heated from all sides by a constant heating source of 1200°C. The temperature for a particular cell in the middle of the tube is recorded. Since it is simply a heat conduction problem with no fluid velocities involved we can compare the finite difference results with results obtained from finite element analysis of similar problems with similar boundary conditions. In the beginning the difference in the results given by the two techniques vary greatly but in the end they both converge and show a steady state is reached after passage of some time. One reason for this difference may be due to the fact that an explicit time marching scheme is used with a coarser mesh in finite difference method while, implicit or Garlerkin schemes are used in the finite element method. The convergence of results from both techniques indicate that the results obtained from finite difference method are reasonable under certain conditions.

APPENDIX B

COMPUTER PROGRAM SOLA

```
      PROGRAM SOLA
*
*P*   NAME:          A NUMERICAL SOLUTION ALGORITHM FOR TRANSIENT
*,*                  FLUID FLOWS
*,*
*,*   DESCRIPTION:
*,*
*,*   AUTHOR:        MODIFIED BY KHALID M. CHAUDHRY
*,*
*,*   DATE:          SEPTEMBER, 1987
*,*
*,*
      IMPLICIT REAL*8 (A-H,O-Z)
***
      DIMENSION  U(400,400), V(400,400), UN(400,400), VN(400,400),
     1 P(400,400), XPUT(400), TEMP(400,400), TEMPN(400,400)


      INTEGER
     1    CYCLE, WL, WR, WT, WB
*
*************************************************
*          OPEN INPUT AND OUTPUT FILES
*************************************************
        CALL UNIOUT
*
        READ (5,*) NUM
        READ (5,*) IBAR,JBAR,WL,WR,WT,WB
        READ (5,*) (XPUT(I),I=1,NUM)
***
       DELX  = XPUT(1)
       DELY  = XPUT(2)
       DELT  = XPUT(3)
       VISC  = XPUT(4)
       CYL   = XPUT(5)
       EPSI  = XPUT(6)
       DZRO  = XPUT(7)
       GX    = XPUT(8)
       GY    = XPUT(9)
       UI    = XPUT(10)
       VI    = XPUT(11)
       TEMPI = XPUT(12)
       TTOP  = XPUT(13)
       TWFIN = XPUT(14)
       UTOP  = XPUT(15)
       PRTLNO= XPUT(16)
       OMG   = XPUT(17)
       ALPHA = XPUT(18)
       TWPRT = XPUT(19)
       VTOP  = XPUT(20)
*
        WRITE(6,20)
        WRITE(6,15) IBAR,JBAR,WL,WR,WT,WB
        WRITE(6,10) (XPUT(I),I=1,NUM)
*********************************************************************
*      COMPUTE CONSTANT TERMS AND INITIALIZE NECESSARY VARIABLES
*********************************************************************
*
       IMAX = IBAR+2
        JMAX = JBAR+2
         IM1 = IMAX-1
          JM1 = JMAX-1
           RDX = 1.0/DELX
```

```
            RDY = 1.0/DELY
             IM2 = IMAX-2
              JM2 = JMAX-2
               T   = 0.
                ITER = 0
                 CYCLE = 0
                  BETA = OMG/(2.*DELT*(RDX**2+RDY**2))
*************************************************************
*     SET INITIAL VELOCITY FIELD INTO U AND V ARRYS
*
*************************************************************
          DO 560 I = 2,IM1
            DO 550 J = 2, JM1
             U(I,J)  = UI
              V(I,J)  = VI
               TEMP(I,J) =TEMPI
550           CONTINUE
560         CONTINUE
*
            GO TO 2000
*****************************************************
*        START CYCLE
*****************************************************
1000    CONTINUE
         ITER = 0
          FLG = 1.
*****************************************************
*      COMPUTE TEMPORARY " U " & " V "
*****************************************************
        DO 1200 I = 2,IM1
         DO 1100 J = 2,JM1
*
       FUX=((UN(I,J)+UN(I+1,J))*(UN(I,J)+UN(I+1,J))+ALPHA*ABS(UN(I,J)+UN(
      1I+1,J))*(UN(I,J)-UN(I+1,J))-(UN(I-1,J)+UN(I,J))*(UN(I-1,J)+UN(I,J)
      2)-ALPHA*ABS(UN(I-1,J)+UN(I,J))*(UN(I-1,J)-UN(I,J)))/(4.*DELX)
*
       FUY=((VN(I,J)+VN(I+1,J))*(UN(I,J)+UN(I,J+1))
      1+ALPHA*ABS(VN(I,J)+VN(I+1,J))*(UN(I,J)-UN(I,J+1))
      2-(VN(I,J-1)+VN(I+1,J-1))*(UN(I,J-1)+UN(I,J))
      3-ALPHA*ABS(VN(I,J-1)+VN(I+1,J-1))*(UN(I,J-1)-UN(I,J)))/(4.*DELY)
*
       FUC=CYL*((UN(I,J)+UN(I+1,J))*(UN(I,J)+UN(I+1,J))+(UN(I-1,J)+UN(I,J
      1))*(UN(I-1,J)+UN(I,J))
      2+ALPHA*ABS(UN(I,J)+UN(I+1,J))*(UN(I,J)-UN(I+1,J))
      3+ALPHA*ABS(UN(I-1,J)+UN(I,J))*(UN(I-1,J)-UN(I,J)))
      4/(8.*DELX*FLOAT(I-1))
*
       FVX=((UN(I,J)+UN(I,J+1))*(VN(I,J)+VN(I+1,J))+ALPHA*ABS(UN(I,J)+UN(
      1I,J+1))*(VN(I,J)-VN(I+1,J))-(UN(I-1,J)+UN(I-1,J+1))*(VN(I-1,J)+VN(
      2I,J))-ALPHA*ABS(UN(I-1,J)+UN(I-1,J+1))*(VN(I-1,J)-VN(I,J)))/(4.*DE
      3LX)
*
       FVY=((VN(I,J)+VN(I,J+1))*(VN(I,J)+VN(I,J+1))+ALPHA*ABS(VN(I,J)+VN
      1(I,J+1))*(VN(I,J)-VN(I,J+1))-(VN(I,J-1)+VN(I,J))*(VN(I,J-1)+VN(I,J
      2))-ALPHA*ABS(VN(I,J-1)+VN(I,J))*(VN(I,J-1)-VN(I,J)))/(4.*DELY)
*
       FVC=CYL*((UN(I,J)+UN(I,J+1))*(VN(I,J)+VN(I+1,J))+(UN(I-1,J)+UN(I-1
      1,J+1))*(VN(I-1,J)+VN(I,J))+ALPHA*ABS(UN(I,J)+UN(I,J+1))*(VN(I,J)-V
      2N(I+1,J))+ALPHA*ABS(UN(I-1,J)+UN(I-1,J+1))*(VN(I-1,J)-VN(I,J)))
      3/(8.*DELX*(FLOAT(I-1)-0.5))
*
       VISX= VISC*((UN(I+1,J)-2.*UN(I,J)+UN(I-1,J))/DELX**2+
      1          (UN(I,J+1)-2.*UN(I,J)+UN(I,J-1))/DELY**2
```

```
     2   +CYL*((UN(I+1,J)-UN(I-1,J))/(2.*DELX*DELX*FLOAT(I-1))
     3   -UN(I,J)/(DELX*FLOAT(I-1))**2))
*
      VISY= VISC*((VN(I+1,J)-2.*VN(I,J)+VN(I-1,J))/DELX**2+
     1          (VN(I,J+1)-2.*VN(I,J)+VN(I,J-1))/DELY**2
     2    +CYL*(VN(I+1,J)-VN(I-1,J))/(2.*DELX*DELX*(FLOAT(I-1)-0.5)))
*
        A = ((UN(I-1,J)*TEMPN(I-1,J))-(UN(I+1,J)*TEMPN(I+1,J)))/DELX
        B = ((VN(I,J-1)*TEMPN(I,J-1))-(VN(I,J+1)*TEMPN(I,J+1)))/DELY
        C = (TEMPN(I+1,J)+TEMPN(I-1,J)-2*TEMPN(I,J))/(DELX**2)
        D = (TEMPN(I,J+1)+TEMPN(I,J-1)-2*TEMPN(I,J))/(DELY**2)

       TEMP(I,J) = TEMPN(I,J)+DELT*(A+B+(VISC*(C+D)/PRTLNO))
*
      U(I,J)=UN(I,J)+DELT*((P(I,J)-P(I+1,J))*RDX+ GX-FUX-FUY-FUC+VISX)
      V(I,J)=VN(I,J)+DELT*((P(I,J)-P(I,J+1))*RDY+ GY-FVX-FVY-FVC+VISY)
1100    CONTINUE
1200   CONTINUE
***************************************************************
*  SET BOUNDRY CONDITIONS FOR 'WL' & 'WR' AND TEMPERATURE.
***************************************************************
2000   CONTINUE
        DO 2200 J = 1,JMAX
          GO TO (2020,2040,2060,2080) WL
2020       U(1,J)=0.0
           V(1,J)=V(2,J)
           TEMP(1,J)= TEMP(2,J)
           GO TO 2100
**
2040       U(1,J)=0.0
           V(1,J)=-V(2,J)
           TEMP(1,J)=tempi
           GO TO 2100
**
2060       IF(ITER .GT. 0) GO TO 2100
           U(1,J)= U(2,J)
           V(1,J)= V(2,J)
           GO TO 2100
**
2080       U(1,J)= U(IM2,J)
           V(2,J)= V(IM1,J)
           V(1,J)= V(IM2,J)
           P(2,J)= P(IM1,J)
2100       GO TO (2120,2140,2160,2180) WR
**
2120       U(IM1,J)=0.0
           V(IMAX,J)=V(IM1,J)
           TEMP(IMAX,J)= TEMP(IM1,J)
           GO TO 2200
**
2140       U(IM1,J)=0.0
           V(IMAX,J)=-V(IM1,J)
           TEMP(IMAX,J)=Tempi
           GO TO 2200
**
2160       IF(ITER .GT. 0) GO TO 2200
           U(IM1,J)=U(IM2,J)*(IM2/IM1*CYL+(1.0-CYL))
           V(IMAX,J)= V(IM1,J)
           GO TO 2200
**
2180       U(IM1,J)=U(2,J)
           V(IMAX,J)=V(3,J)
2200    CONTINUE
```

```
************************************************
*  NOW FOR 'WT' &'WB' AND TEMPERATURE.
************************************************
       DO 2500 I = 1,IMAX
         GO TO(2320,2340,2360,2380) WT
2320     V(I,JM1)= 0.0
         U(I,JMAX) = U(I,JM1)
         TEMP(I,JMAX)= TEMP(I,JM1)
         GO TO 2400
**
2340     V(I,JM1)   =  0.0
         U(I,JMAX)  =  -U(I,JM1)
         TEMP(I,JMAX)= TEMP (I,JM1)
         GO TO 2400
**
2360     IF(ITER .GT. 0) GO TO 2400
         V(I,JM1)= V(I,JM2)
         U(I,JMAX)=U(I,JM1)
         TEMP (I,JMAX) = TEMP (I,JM1)
         GO TO 2400
**
2380     V(I,JM1)=V(I,2)
         U(I,JMAX)=U(I,3)
**
2400     GO TO(2420,2440,2460,2480) WB
**
2420     V(I,1) = 0.0
         U(I,1) = U(I,2)
         TEMP(I,1)=Ttop
         GO TO 2500
**
2440     V(I,1)=0.0
         U(I,1)=-U(I,2)
         TEMP(I,1)=TTOP
         GO TO 2500
**
2460     IF(ITER .GT. 0) GO TO 2500
         V(I,1)=V(I,2)
         U(I,1)=U(I,2)
         GO TO 2500
**
2480     V(I,1)=V(I,JM2)
         U(I,2)=U(I,JM1)
         U(I,1)=U(I,JM2)
         P(I,2)=P(I,JM1)
2500   CONTINUE
****************************************
*    SPECIAL BOUNDARY CONDITION.
****************************************
          IF ( TTOP .NE. 0.) THEN
             DO 2800 I = 1,IMAX
2800         TEMP(I,1)= TTOP
           ELSE
           ENDIF
*
           IF( UTOP .NE. 0.) THEN
             DO 2810 I = 1,IMAX
2810         U(I,1)= UTOP
           ELSE
           ENDIF
*
           IF( VTOP .NE.0.) THEN
             DO 2820 I = 1,IMAX
```

```
2820          V(I,1) = VTOP
             ELSE
            ENDIF
*
             IF( CYCLE .LE. 0) THEN
              GO TO 5600
              ELSE
              ENDIF
3000         CONTINUE
*****************************************
*     HAS CONVERGENCE REACHED?
*****************************************
        IF ( FLG .EQ. 0.) GO TO 5600
        ITER = ITER+1
        IF ( ITER .LT. 500) GO TO 3050
        IF ( CYCLE .LT. 10) GO TO 5600
        T = 1.E+10
        GO TO 5600
3050    FLG = 0.0
*****************************************************************
*   COMPUTE UPDATED CELL PRESSURES, VELOCITIES, TEMPERATURES
*****************************************************************
        DO 3500 J = 2,JM1
         DO 3200 I = 2,IM1
          D=RDX*(U(I,J)-U(I-1,J))+RDY*(V(I,J)-V(I,J-1))+CYL*(U(I,J)
     1    +U(I-1,J))/(2.*DELX*(FLOAT(I)-1.5))
          IF (ABS(D/DZRO) .GE. EPSI) FLG=1.0
           DELP = -BETA*D
            P(I,J) = P(I,J)+DELP
            U(I,J) = U(I,J)+DELT*RDX*DELP
            U(I-1,J) = U(I-1,J)-DELT*RDX*DELP

*
            V(I,J)= V(I,J)+DELT*RDY*DELP
            V(I,J-1)= V(I,J-1)-DELT*RDY*DELP
3200     CONTINUE
3500    CONTINUE
         GO TO 2000
*************************************
5600    CONTINUE
*
        IF(T .GE. TWPRT ) THEN
         WRITE(6,30) ITER, T, CYCLE
          WRITE(6,40)
          DO 5900 I= 1,IMAX
           DO 5850 J= 1,JM1
            WRITE(6,50) I, J, U(I,J), V(I,J), P(I,J), TEMP(I,J)
5850        CONTINUE
5900     CONTINUE
         ELSE
        ENDIF
*************************************************************
*   SET THE ADVANCE TIME ,VELOCITIES AND TEMPERATURE
*************************************************************
6000     CONTINUE
         DO 6200 I=1,IMAX
          DO 6100 J=1,JMAX
          UN(I,J) = U(I,J)
          VN(I,J) = V(I,J)
          TEMPN(I,J) = TEMP(I,J)
6100       CONTINUE
6200     CONTINUE
*****************************************************
```

```
*       ADVANCE TIME, T=T+DELT
*******************************************************
            T = T+DELT
            IF( T .LE. (TWFIN+DELT)) THEN
             CYCLE = CYCLE+1
             GO TO 1000
             ELSE
            ENDIF
6500         CONTINUE
*******************************************************
*     WRITE ALL FORMAT STATEMENTS
*******************************************************
*
10     FORMAT(5X,'DELX=',F10.5
     1/5X,'DELY=',F10.5/5X,'DELT=',F10.5/5X,'NU=',F13.5/5X,'CYL=',
     2F12.5/5X,'EPSI=',F10.5/5X,'DZRO=',F10.5/5X,'GX=',F13.5/5X,'
     3GY=',F13.5/5X,'UI=',F13.5/5X,'VI=',F13.5/5X,'TEMPI=',F10.5/5X
     4,'TTOP=',F10.5/5X,'TWFIN=',F10.5/5X,'UTOP=',F10.5/5X,'PRTLNO=',
     5F9.5/5X,'OMG=',F12.5/5X,'ALPHA=',F10.5/5X,'TWPRT=',F10.5/5X,'VT
     6OP=',F10.5/)
*
20      FORMAT(/20X,' INITIAL INPUT DATA',/)
*
15      FORMAT(5X,'IBAR=',I5/5X,'JBAR=',I5/5X,'WL=',I7/5X,'WR=',I7/5X,'
     1WT=',I7/5X,'WB=',I7)
*
30      FORMAT(/5X,'ITER=',I3,10X,'TIME=',F12.5,6X,'CYCLE=',I3)
*
40      FORMAT(/4X,'I',4X,'J',9X,'U',12X,'V',12X,'P',10X,'TEMP',/)
*
50      FORMAT(2X,I3,2X,I3,2(1X,F12.2),1X,F12.2,1X,F12.2)
*
1       FORMAT(5X,'A=',F12.5,5X,'B=',F12.5,/5X,'C=',F12.5,5X,'D=',F12.5,/
     15X,'TEMPn=',F12.5,5x,'temp=',f12.5)
        STOP
         END
```